ISSN 2635-1676, Nanobiotechnology Reports, 2022, Vol. 17, No. 3, pp. 261–289. © Pleiades Publishing, Ltd., 2022.

REVIEWS

Ultra-Sensitive Magnetoelectric Sensors of Magnetic Fields for Biomedical Applications

A. V. Turutin[a,*], I. V. Kubasov[a], A. M. Kislyuk[a], V. V. Kuts[a], M. D. Malinkovich[a], Yu. N. Parkhomenko[a,b], and N. A. Sobolev[a,c]

[a] *National University of Science and Technology MISiS, Moscow, 119049 Russia*

[b] *AO State Research and Design Institute of Rare-Metal Industry "Giredmet", Moscow, 111524 Russia*

[c] *Department of Physics, University of Aveiro, Aveiro, Portugal*

**e-mail: aturutin92@gmail.com*

Received August 26, 2021; revised August 26, 2021; accepted February 11, 2022

Abstract—Composite multiferroics are materials in which electric polarization of the material is possible under the action of an external magnetic field and vice versa, a change in the magnetization of the structure when an electric field is applied. Such properties have a high practical potential for application in science and technology. Based on these materials, it is possible to manufacture a number of devices with unique properties, such as, for example, random access magnetoelectric (ME) memory, ME sensors of magnetic fields, current, magnetic nanoparticles, micromechanical ME antennas, voltage-adjustable microwave filters, resonators and phase shifters. Therefore, the search for new materials of composite multiferroics and the study of the ME effect in them is a priority and urgent task in the search and creation of new electronic devices. One of the most promising and close to practical implementation directions is the creation of highly sensitive sensors of ultra-weak magnetic fields on the basis of composite multiferroics. The absence of the need to cool such sensors is a significant technical advantage over superconducting quantum interferometers currently used for these purposes. To date, the best achieved limits for detecting magnetic fields using sensors based on composite magnetoelectrics are values of the order of $pT/Hz^{1/2}$, and new works are regularly published that reduce this threshold by improving processing electronics and changing the sensor design. This threshold of sensitivity is already sufficient for reliable detection of magnetic fields induced by alpha-rhythm currents of the brain with amplitudes of units of pT (magnetoencephalography) and for detecting the magnetic activity of the human heart. The review article is devoted to composite magnetoelectric structures with a focus on sensor structures capable of detecting ultra-weak magnetic fields. The comparison of the limiting sensitivity to the magnetic field of the existing ME composite structures is carried out, the ways of increasing the sensitivity to the magnetic field are shown.

DOI: 10.1134/S2635167622030223

CONTENTS

INTRODUCTION

Composite multiferroics are structures in which ferromagnetic and ferroelectric ordering exist simultaneously [1]. The magnetoelectric (ME) effect in composite multiferroics occurs due to an elastic bond between magnetostrictive and piezoelectric materials. The term "ME effect" in the most general sense describes the effect of change in magnetization on the electrical polarization of a sample (direct ME effect) and, on the contrary, the effect of change in electrical polarization on magnetization (reverse ME effect) [2].

At present, there is a significant spike in publication activity on topics devoted to the production and study of the properties of composite multiferroics. Particularly, a search using the key words "composite multiferroic" in the Web of Science Core Collection scientometric database demonstrates a stable annual increase in the number of publications and citations by 10–15% since 2010. Such interest in composite multiferroics is primarily associated with the possibility of fabricating a number of devices with unique properties on their basis, such as, for example, microwave phase shifters, electronically adjustable microwave resonators and delay lines, waste thermal energy collection systems, energy-independent ME memory, microme-

chanical ME antennas, ME gyrators, and ultra-sensitive sensors of magnetic fields (MF) [2–6]. It was demonstrated that layered ME composites containing mechanically connected magnetostrictive and piezoelectric layers parallel to each other are able to generate a large electrical signal in response to weak changes in an external MF [2, 4, 7–9].

The creation of highly sensitive sensors of ultra-weak MFs based on composite multiferroics is one of the directions that are most promising and close to practical implementation [10–12]. The lack of the necessity to cool such sensors is a significant technical advantage over superconducting quantum interference devices (SQUIDs) used now for these purposes without alternative. It is obvious that MF sensors based on composite multiferroics cannot completely replace SQUIDs, which are capable of detecting individual quanta of a magnetic flux [13]; however, there are a number of applications, in which the use of MF sensors based on composite multiferroics (not requiring cooling to cryogenic temperatures) is justified. Such areas of application include highly sensitive miniature magnetometers of industrial and research classes for the contactless measurement of ultra-weak currents, MFs in living organisms applied to magnetocardiography and magnetoencephalography, the visualization of magnetic nanoparticles, the measurement of magnetic anomalies, magnetic geological exploration, etc.

To date, a limit of MF detection on the order $pT/Hz^{1/2}$ has been achieved using sensors based on composite multiferroics; moreover, new works are regularly published, where this threshold is lowered due to improvement in the processing electronics and a change in the design of such sensors [10, 14, 15]. Such a threshold of sensitivity is sufficient for detecting MF induced by α-rhythm currents of the brain with amplitudes of units of pT (magnetoencephalography) and currents flowing in the human heart (magnetocardiography) [11, 16]. On the other hand, it is necessary to be able to measure MFs with a magnitude 1–2 orders of magnitude lower with a high degree of reliability to study the activity of the cerebral cortex. At present, such levels of sensitivity of a sensor based on a composite multiferroic have not been implemented by any research team around the world.

To achieve a high sensitivity to MFs at low frequencies, ME sensors must have a large coefficient of conversion of MF into electrical field, as well as low internal and external noise levels. The overwhelming majority of research teams involved in the production and study of the properties of composite multiferroics use materials based on piezoceramics of PZT (lead zirconate titanate) type or relaxor ferroelectrics of PMN-PT (lead magnesium niobate–lead titanate) type in their research. Despite outstanding piezoelectric characteristics, these materials have a number of disadvantages, such as a low Curie temperature, significant mechanical-electrical hysteresis, creep (time delay between the mechanical deformation and electrical signal) and saturation, nonlinear dependence of the properties on temperature, and large dielectric losses. Being multicomponent solid solutions, the substances mentioned above can differ greatly in their properties for different manufacturers, while control of the ferroelectric domain structure and electrical conductivity becomes a difficult technical challenge. The use of PZT-type piezoelectric ceramics and PMN-PT-type ferroelectric relaxors with high values of piezoelectric modules d_{ij} allows a significant increase in the coefficient of conversion of mechanical deformation into an electrical signal; but at the same time, due to the huge values of the dielectric permittivity ε and, consequently, large capacity, the voltage generated by the piezoelectric effect will be relatively low. Thus, the efficiency of conversion of mechanical deformation into an electrical signal is particularly determined by d/ε ratio [15, 17].

The use of piezoelectric single crystals with average values of piezoelectric modules, but with low mechanical and dielectric losses, is a promising approach for obtaining large coefficients of conversion of MF energy into an electrical signal. Single crystals of classical 180° ferroelectrics, such as, for example, lithium niobate ($LiNbO_3$, LN) and lithium tantalate ($LiTaO_3$, LT), are an interesting variant for this purpose [18, 19]. These materials demonstrate excellent temperature stability, have high Curie temperatures (1140°C in LN and 620°C in LT), have no creep and no mechanical-electrical hysteresis [20]. At the same time, being primarily materials for laser optics and acoustics, lithium niobate and lithium tantalate are produced by industry in large volumes and have excellent reproducibility of properties.

The sensitivity of a ME sensor is mainly limited by its own noise, in which Nyquist thermal noise and 1/f noise dominate [2, 17]. The thermal noise can be minimized due to the use of appropriate detection schemes of weak output signal from ME structures [21]. Suitably designed schemes of detection based on voltage or charge amplifiers must have a noise amplitude on the level of the sensitivity limit of these components [22, 23]. On the other hand, external noise caused by vibrations of the piezoelectric, pyroelectric noise and magnetic sources of noise require more complex strategies to deal with them [10, 24, 25].

It is known that asymmetrical two-layer systems containing a mechanical-electrical transducer of the bimorph type demonstrate especially large ME coefficients with a bending resonance [26–29]. At the same time, it is possible to fasten the bimorph as a cantilever for a significant increase in the ME effect at low frequencies [10]. In addition to an increase in the sensi-

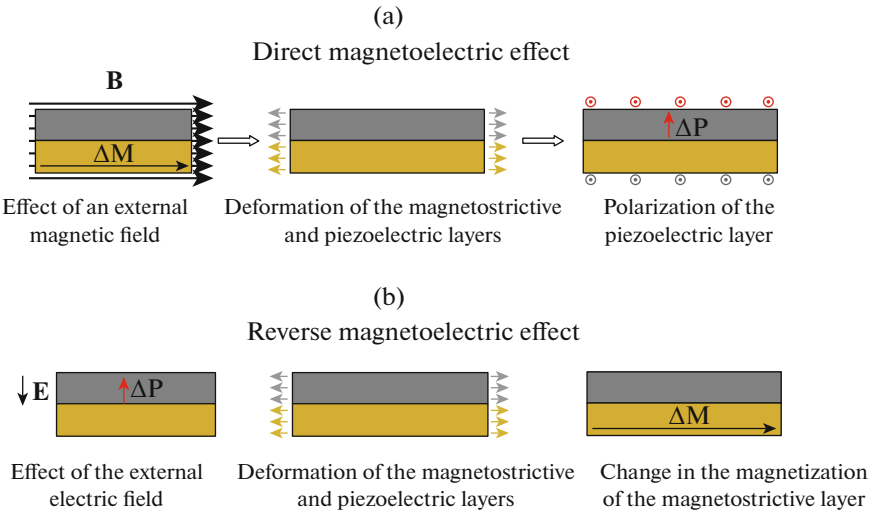

Fig. 1. Schematic image of the ME effect arising as a result of deformation of one of the layers (magnetostrictive or piezoelectric layer): (a) direct ME effect, (b) reverse ME effect.

tivity at low frequencies and an increase in the ME coefficient, such a configuration can partially compensate the vibration and thermal noise [17, 30].

Bimorph piezoelectric structures are usually made by gluing or sintering together piezoelectric plates based on PZT [26, 31, 32]. As a rule, such a method leads to the appearance of interphase boundaries and adhesive layers, resulting in large mechanical losses and instability of the material properties. From this point of view, the advantage of LN and LT consists in the possibility of obtaining single-crystal bimorphs (containing no adhesive layer or intercrystalline boundary) on their basis due to the creation of counter-polarized bidomain ferroelectric structures of "head-to-head" and "tail-to-tail" types [33]. Bidomain crystals are obtained using pulsed infrared annealing accompanied by the emergence of a given temperature gradient in the sample volume and, as a consequence, internal electric field polarizing the domains towards each other [20, 34]. The use of a bidomain crystal as the piezoelectric part of a composite multiferroic prevent the losses associated with the sintering or adhesion boundary in the piezoelectric material.

This review is devoted to composite ME structures with a focus on sensor structures capable of detecting ultra-weak MFs. In particular, their use in the field of human-heart MF detection is demonstrated.

1. ME EFFECT IN COMPOSITE STRUCTURES

According to the initial definition proposed by Debye in 1926 [35], the linear ME effect is described as the appearance of electric polarization (P) of a sample when applying a magnetic field (H) to it. This phenomenon is called the direct ME effect. There is also a reverse ME effect, which is determined as the appearance of magnetization (M) of the sample when applying an electric field (E) to it. Illustration of this effect for the composite structure is given in Fig. 1 [36].

The direct and reverse linear ME effects can be expressed by the formulas [1, 37]:

$$P_i = \alpha_{ij} H_j, \quad (1)$$

$$M_i = \alpha_{ji}/\mu_0 E_j, \quad (2)$$

where α_{ij} is a linear ME coefficient; P_i is the vector of polarization of a material; M_i is the vector of magnetization of a material; H_j is the vector of the MF strength; E_j is the vector of the electric-field strength; μ_0 is the magnetic permeability of free space. Here and below, the Einstein summation is used.

The association of the polarization vector **P**, material magnetization vector **M**, vector of the electric field strength **E**, and the magnetic-field strength **H** can be graphically shown as a diagram (Fig. 2).

In order to understand better the appearance of the ME effect in composite structures, we consider the concept of physical properties that appear as a result of a combination of different single-phase compounds. As is known, composite systems can not only have properties similar to those of their constituent phases, but also have completely new properties that are absent in the initial compounds. While summary and proportional properties determine averaging or amplification of the effect, multiplicative properties lead to new effects formed from interaction between the materials that form the composite [38]. Multiplicative properties are used to create structures that have the ME effect from materials that do not.

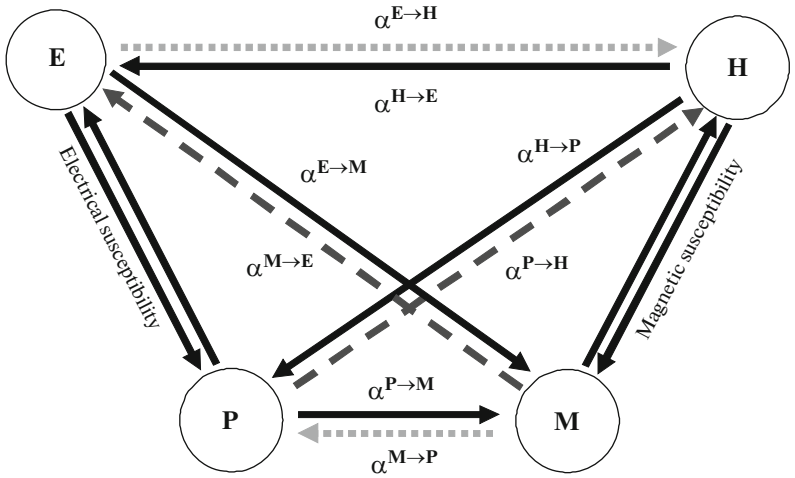

Fig. 2. Magnetoelectric coefficients and their reverse values [37]. Image copied with permission WILEY © 2021.

The ME effect in composite multiferroics emerges due to the interaction between piezoelectric and magnetostrictive phases [4, 38, 39]. The direct ME effect in such composite system emerges when applying a MF to samples. The applied MF deforms the magnetostrictive material, which leads to mechanical deformation of the piezoelectric material, which is polarized due to the direct piezoelectric effect (Fig. 1a).

Qualitatively, the direct and reverse ME effects in the composite structures can be described by the expressions [39]:

$$\mathrm{ME}_H\ \text{effect} = \frac{\text{Electrical}}{\text{Mechanical}} \times \frac{\text{Mechanical}}{\text{Magnetic}}, \quad (3)$$

$$\mathrm{ME}_E\ \text{effect} = \frac{\text{Magnetic}}{\text{Mechanical}} \times \frac{\text{Mechanical}}{\text{Electrical}}, \quad (4)$$

where the ratio of properties electrical/mechanical is the generation of a piezoelectric charge ($d_{ij} = \partial D_i/\partial T_j$); mechanical/magnetic is deformation due to the effect of magnetostriction ($q_{ij} = \partial S_j/\partial H_i$); magnetic/mechanical is piezomagnetic induction ($q_{ij} = \partial B_i/\partial T_j$); and mechanical/electrical is piezoelectric deformation ($d_{ij} = \partial S_j/\partial E_i$).

Within this concept, provided that $E_i = 0$, the effective ME coefficient can be expressed according to [40]:

$$\begin{aligned}\alpha_{ij} &= k_c(\partial P_i/\partial H_j) \\ &= k_c(\partial P_i/\partial S_k)(\partial S_k/\partial H_j) = k_c d_{ik} q_{jk},\end{aligned} \quad (5)$$

where k_c is the coupling coefficient ($0 \le |k_c| \le 1$), which quantitatively determines the efficiency of the transfer of deformation between the phases of a composite material; d_{ik} is the piezoelectric coefficient; and q_{jk} is the piezomagnetic coefficient.

Thus, the composite structure has the ME effect, which is not observed in individual phases of these materials.

We consider the types of compounds in composite structures. Using the Newman concept [41, 42] to describe structures consisting of different phases, ME composites can be divided into three main types. In this case, the following designations are used: 0 is single-phase particles suspended in a matrix of another phase, which is designated by number 3; 1 is single-phase fibers; and 2 is films or layers of one of the phases. The designations 0–3, 2–2, and 1–3 are used to describe the structures of composite ME materials, where each number designates the connection with the material phase (Fig. 3). Composites of 0—3 and 1—3 types demonstrate low values of the ME effect (no more than 500 mV/(cm Oe)) due to high leakage currents through ferromagnetic inclusions and dissipation of the energy of mechanical vibrations of the magnetostrictive phase on an epoxy film, which binds the ferroelectric and magnetic phases [36, 43–45]. In horizontal heterostructures of the type 2–2 with a layered structure, there are no problems with leakage currents due to a high resistance of the ferroelectric layer. Each of the layers is produced in an independent technological process, which increases the number of possible parameters, using which it is possible to influence the value of the ME effect in the composite structure. The largest ME effect was observed namely in type 2–2 structures, which can be seen in the diagram given in Fig. 4 [7]. The best experimental values of the quasistatic ME coefficient, obtained for different combinations of materials in bulk and film ME composites having a connection of the 0–3, 1–3, and 2–2 types, are collected in [7].

The direct and reverse ME effects can be applied in a wide range of new devices. Table 1 gives the main

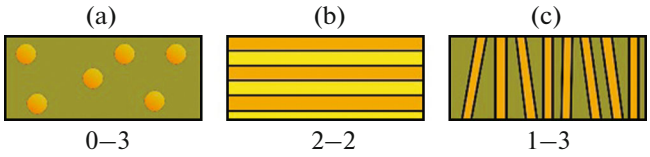

Fig. 3. Schematic image of the three most common types of ME structure connections: (a) 0–3, composite films consisting of a piezoelectric matrix (3), in the structure of which magnetic particles (0) are introduced; (b) 2–2, horizontal heterostructure with alternating ferroelectric (2) and magnetic (2) layers; (c) 1–3, vertical heterostructure with fibers of magnetic (or ferroelectric) material introduced into the matrix of the ferroelectric (or magnetic) material in the form of columns.

types of ME devices and their classification relative to the ME effect, and references to recent scientific works and reviews on this topic.

2. ME EFFECT IN COMPOSITE MULTIFERROICS

In the overwhelming majority of works devoted to studying the ME effect in composite multiferroics, a technique for measuring the ME coefficient by the dynamic method is used [79–82]. The idea of the method is to measure the effective value of a small variable electrical voltage (V_{out}) arising on the sample, when applying a small variable MF (δH) to it. The value of the ME coefficient can be obtained from the expression $\alpha_{ME} = V_{out}/(t\delta H)$, where t is the thickness of the piezoelectric layer of the composite ME material. The following devices are used to realize the dynamic method: a lock-in (or oscillograph), signal generator, Helmholtz coils (solenoid, electromagnet), current amplifier, and multimeter. The variant of realization of this system is presented in Fig. 5. Such a system allows information to be obtained about the effect of a number of parameters (materials of the composite structure, connection between the components in the composite structure, mode of operation of the ME sample, methods of obtaining materials, etc.) on the value of the ME effect, as well as ME materials most suitable for different applications to be identified.

This method also allows measurement of the phase shift of the useful signal relative to the signal applied to the Helmholtz coils and a change in the phase signal from the sample in the process of measurement. By changing the value of a constant MF, it is possible to study the ME effect at different working points of a magnetostrictive material, whereas by changing the frequency of a variable MF, one can study the response of the sample at different frequencies of MFs. Since the variable ME signal of the response from the sample in this method is measured using a synchronous detector in a narrow region near the excitation frequency, the noise and other parasitic interference significantly decrease due to signal filtering both in frequency and in phase [83], which allows weak electric signals from ME samples to be measured.

According to the formula (5), the ME coefficient α_{ME} is proportional to the piezomagnetic coefficient of the magnetostrictive material $q_{ij} = \partial\lambda_{ij}/\partial H$. The magnetostriction coefficient λ_{ij} has a nonlinear dependence on a constant MF for most magnetic materials. A typical dependence of the magnetostriction coefficient on a constant MF for such a class of magnetic materials as amorphous metallic glasses is

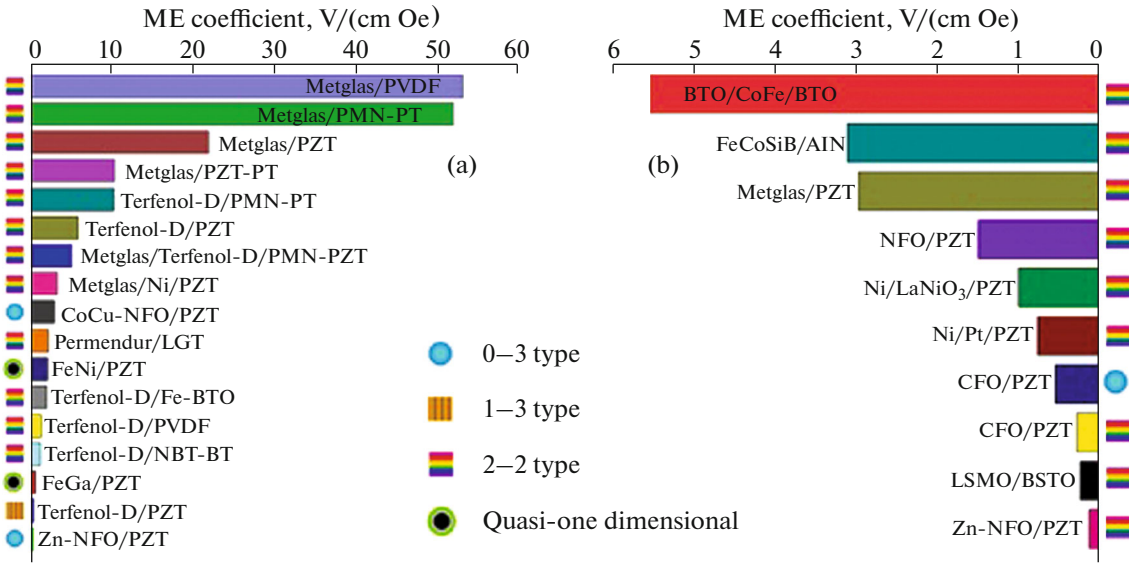

Fig. 4. Values of nonresonance ME coefficients for different materials: on the right bulk and on the left film ME composites [7] (image copied in accordance with the license CC BY 4.0).

Table 1. Use of composite multiferroics

ME effect	Physical mechanism used in devices	Devices
Direct	Change in the electrical polarization of a material when applying a magnetic field	Magnetic sensors [6, 11, 12, 16, 31, 46–50]; current sensors [7, 51–54]; gyrators [55–60]; devices for collecting waste energy [61–65], and detection of magnetic nanoparticles [66]
Reverse	Change in the magnetization of a material by an electric field	Spintronics, including ME memory with random access (MERAM) [36, 40, 67, 68]
	Change in the magnetic permeability μ by an electric field	Voltage-adjustable inductivities [69–71] and bandpass filters [72–74]. Mechanical antennas [75, 76]
	Control of spin waves by an electric field	Voltage-adjustable filters, resonators, phase shifters [6, 70, 72, 77, 78]

presented in Fig. 6a. Thus, there is a constant MF, at which the piezomagnetic coefficient is maximal [84]. The value of this MF is called the working point of the composite ME material, since the maximal ME effect is observed with this MF value.

The dependence of the ME coefficient on a variable MF is another important characteristic of composite multiferroics (Fig. 6b). Depending on the geometry of structures at a certain frequency, a multiple increase in the ME coefficient can be observed, which corresponds to the electromechanical resonance of the sample. The value of the direct ME coefficient reaches a maximum at the antiresonance frequency (f_a) [85].

According to Fig. 4, the largest ME effect is observed in layered composite multiferroics. Such structures can be divided into four main categories depending on how the magnetization (M) of the magnetostrictive layer and polarization (P) of the piezoelectric layer are directed relative to each other. The main four types of structures and three derivatives of them are presented in Fig. 7 [4].

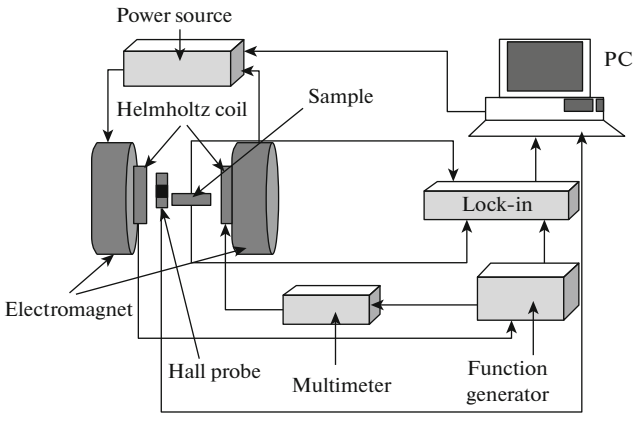

Fig. 5. Measuring systems for the ME effect via the dynamic method using an electromagnet to apply a constant MF to a sample [79] (image copied with permission of Elsevier © 2021).

In the case of piezoelectric ceramics PZT and PMN-PT, it was demonstrated [86] that the maximal ME effect can be obtained for the composite configuration with the structure $L–L$. This is explained by the largest piezoelectric coefficient d_{33} in PZT and PMN-PT. In order to avoid these disadvantages, a modified structure with symmetric polarization of the piezoelectric layer relative to the central line was suggested (Fig. 7d) [30, 87, 88]. This configuration is called *push-pull* [87]. The *push-pull* design allows an increase in the value of the removed voltage by 2 times as compared with the regular $L–L$-configuration. It was suggested to use a piezo fiber out of PZT with interdigitated (ID) electrodes applied to its surface as a piezoelectric material [89]. Metglas, which was applied using epoxy glue on both sides of the piezoelectric material, was used as the magnetostrictive material. A schematic layered image of the composite structure piezo fiber/Metglas ($L–L$) and measured dependence of the ME coefficient on the frequency of the MF are presented in Fig. 8.

The piezo fiber was made of PZT-5A ceramic with a thickness of 100 μm, width of 350 μm, and length of 30 mm. The Metglas width is 7 mm, and its length is 100 mm. In order to isolate ID electrodes from the conductive Metglas, a polyimide film was formed between them. The piezo fiber consists of a number of alternating symmetrical longitudinally polarized blocks with the length $2l_p = 1$ mm, to which ID electrodes are connected to collect charges (inset in Fig. 8a). Such a configuration increases the structure capacity and optimizes the transmission of mechanical stress [90].

The measurements of ME coefficient of the piezo fiber/Metglas ($L–L$) composite structure depending on the frequency of the MF are given in Fig. 8b. The maximum of the ME coefficient corresponds to electromechanical resonance of the structure at a frequency of 10.5 kHz and is ~470 V/(cm Oe). At a low frequency (in the range from 1 to 1000 Hz), the ME coefficient slightly depends on the MF frequency and is 23 V/(cm Oe). These measurements were carried out when applying the optimal MF (4 Oe). The use of

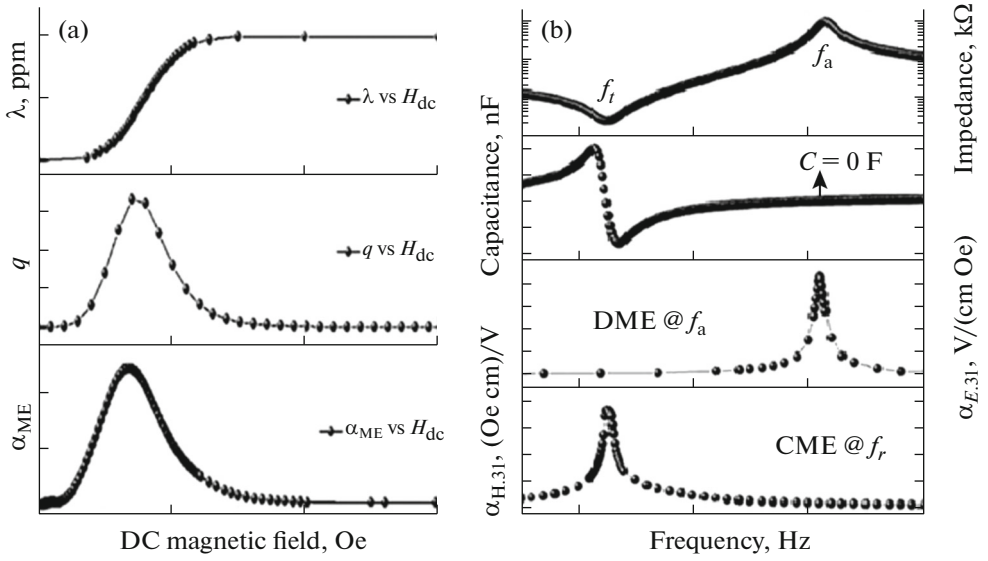

Fig. 6. Typical dependences of magnetostriction, piezomagnetic and ME coefficients on a constant MF (a). Dependencies of the impedance, capacity, direct and reverse ME coefficients on the frequency of a modulating MF for a composite multiferroic (b) [7] (graphs copied in accordance with the license CC BY 4.0).

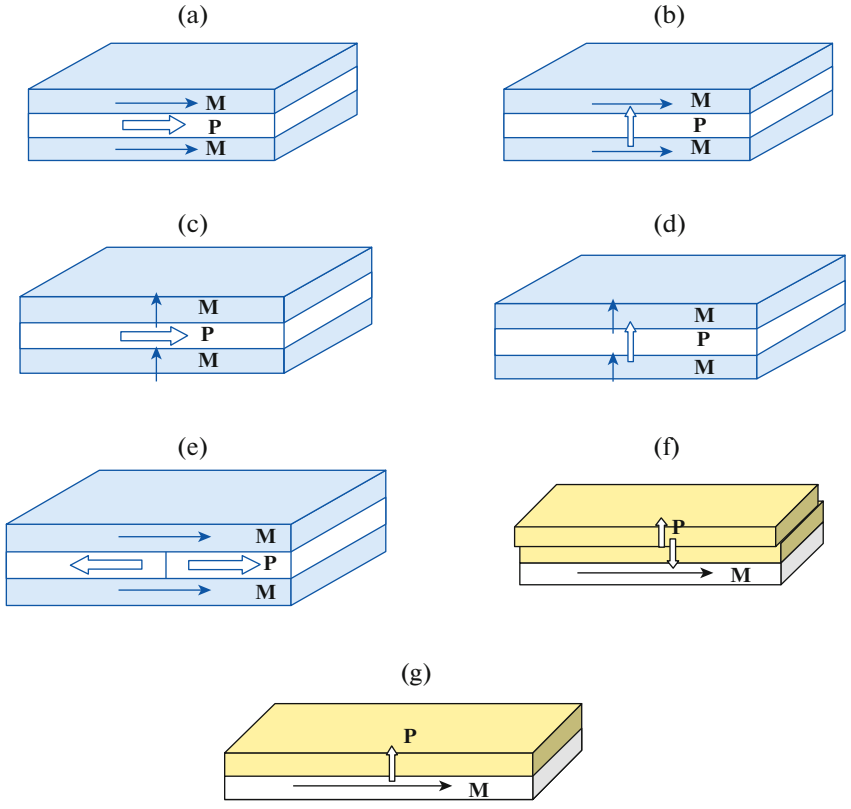

Fig. 7. Schematic image of layered composite materials consisting of magnetostrictive and piezoelectric layers with different direction of the polarization vector (**P**) and magnetization (**M**) with the following configurations of the structures: (a) "longitudinal (**M**)–longitudinal (**P**)" (*L*–*L*); (b) "longitudinal (**M**)– transverse (**P**)" (*L*–*T*); (c) "transverse (**M**)–longitudinal (**P**)" (*T*–*L*); (d) "transverse (**M**)–transverse (**P**)" (*T*–*T*); (e) configuration (*L*–*L*) with symmetrical localization of the piezoelectric (**P**) relative to the central separating line (*push-pull*) [30]; (f) bimorph composite material; (g) single-domain composite material with a single magnetostrictive layer [4] (Figs. 7f and 7g copied with permission of AIP Publishing © 2021).

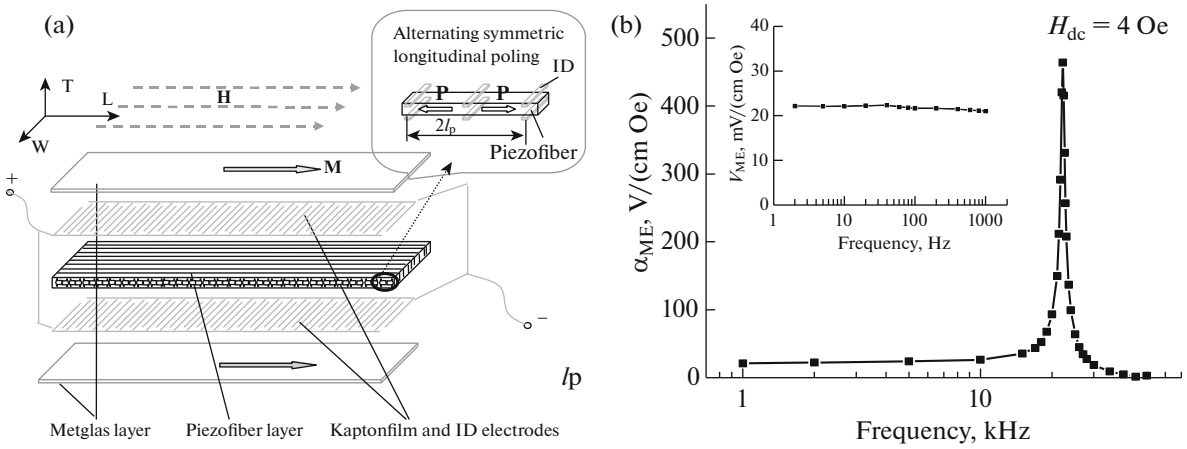

Fig. 8. Layered scheme of a composite multiferroic piezo fiber/Metglas (L–L) (a). Dependence of the ME coefficient on the frequency of the modulating field for this structure (b). Low frequency part of the dependence of the ME coefficient on the frequency of a MF is presented in the insert [89] (graphs copied with permission of AIP Publishing © 2021).

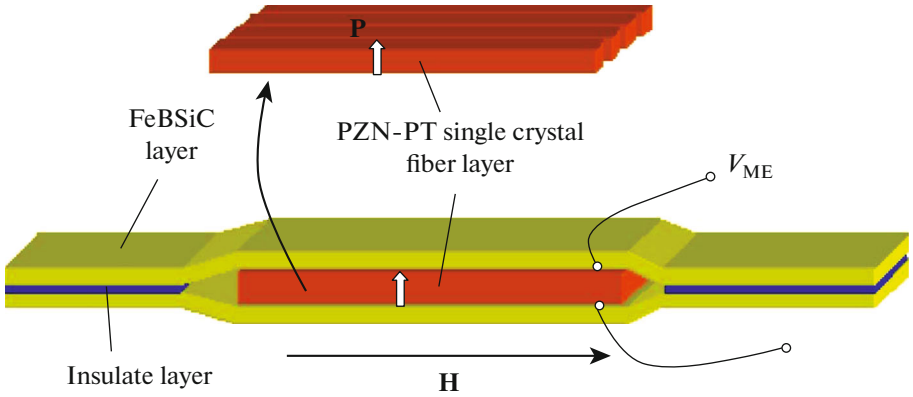

Fig. 9. Composite multiferroic on the basis of a three-layer FeBSiC/PZN-PT piezo fiber/FeBSiC material with L–T construction. The **P** vector designates the direction of polarization in the layer of the PZN-PT piezo fiber [91] (figure copied with permission of AIP Publishing © 2021).

push-pull composite ME materials made it possible to obtain one of the maximal ME coefficients beyond the electromechanical resonance for composite multiferroics.

L–T is another widely used design of ME composite materials. As compared with the L–L-configuration, it is possible to obtain a larger electric capacity of ME structures with the same geometric dimensions, which increases the ME coefficient [91]. The transverse piezoelectric effect is lower than the longitudinal one for almost all materials, which is an advantage for the L–L-configuration.

A composite structure with the L–T design on the basis of Metglas/$Pb(Zn_{1/3}, Nb_{2/3})O_3$–7% $PbTiO_3$ (PZN-PT) was studied in [91]. A schematic image of the composite material layers is presented in Fig. 9.

The commercial amorphous alloy Metglas as the magnetostrictive material and PZN-PT piezofiber crystal polarized along d_{31} as the piezoelectric material were used in the experiment. Magnetostrictive and piezoelectric layers were adhered using epoxy resin. A thin PZN-PT crystal oriented with a long side along the direction [100] was cut in the form of columns with the length 15 mm, width 0.4 mm, and thickness 0.1 mm. Metglas was cut with the length 100 mm, width 5 mm, while its thickness was 25 μm.

Measurements of the ME coefficient in the quasistatic and dynamic modes are presented in Fig. 10.

The maximal value of the quasistatic ME coefficient was 10 V/(cm Oe) at a constant MF of 2 Oe. This effect is only 2 times less than in the structure piezofiber/Metglas (L–L) [89]. However, the dynamic ME coefficient at the frequency of electromechanical resonance (20 kHz) was 400 V/(cm Oe), which is on the same order as the previous result for the configuration (L–L).

In [92], it was suggested to use a PMN-PT crystal doped with Mn with a transverse value of the piezoelectric coefficient d_{31} = 1800 pC/N and very low

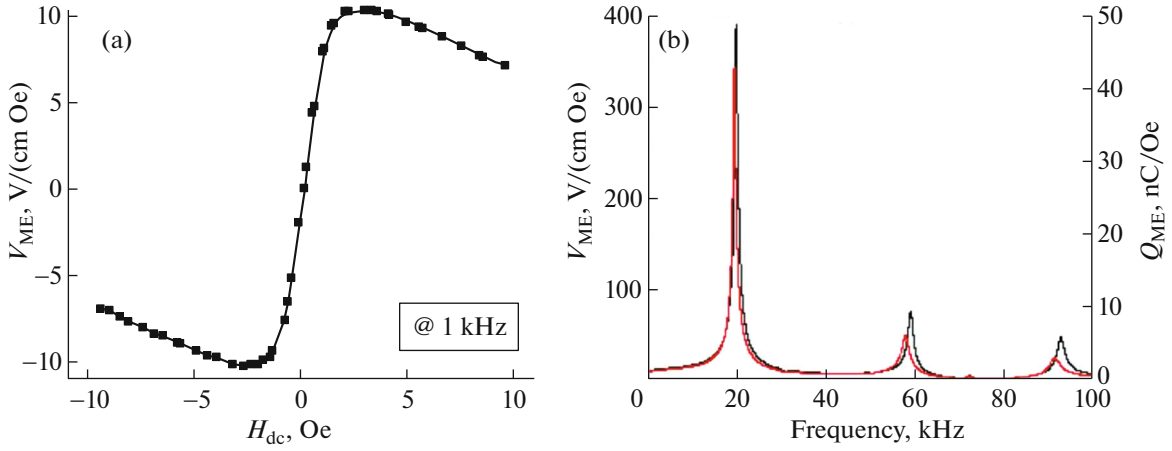

Fig. 10. Dependence of the ME coefficient of a three-layer composite material FeBSiC/PZN-PT piezo fiber/FeBSiC on a constant MF at a frequency of the modulating MF of 1 kHz (a). ME coefficient as a function of the frequency of a variable MF when applying the optimal constant MF $H_{dc} = 2$ Oe (b) [91] (graphs copied with permission of AIP Publishing © 2021).

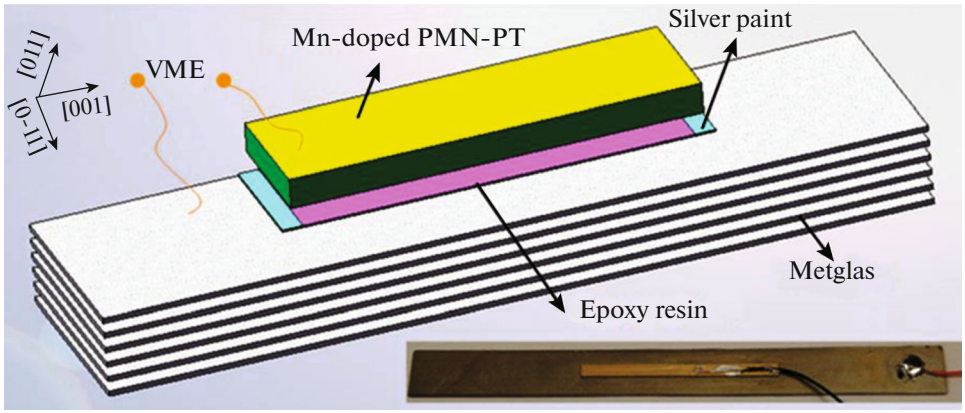

Fig. 11. Schematic image and photo of a composite multiferroic of Metglas/PMN-PT based structure (doped with manganese) [92] (figure copied with permission of AIP Publishing © 2021).

value of the tangent of the dielectric-loss angle $\tan\delta = 0.07\%$ as a piezoelectric component in the composite multiferroic. The sizes of the PMN-PT crystal were $30 \times 2 \times 0.2$ mm^3. Metglas ($Fe_{74.4}Co_{21.6}Si_{0.5}B_{3.3}Mn_{0.1}C_{0.1}$) was selected as the magnetostrictive material. The obtained composite material refers to the $L-T$ configuration. The thickness of the Metglas ribbon is 25 μm, its length is 80 mm, and its width is 8 mm. To increase the ME coefficient, it was suggested in the work to increase the volume of the magnetostrictive phase by gluing together 12 Metglas samples. To create the composite multiferroic, PMN-PT piezoelectric material (doped with Mn) was glued with nonconductive epoxy resin to the prepared multilayer Metglas sample. The layered scheme of the composite material and its photo are given in Fig. 11.

Quasistatic measurements of the ME coefficient depending on the value of the constant MF were conducted when applying a variable MF $H_{ac} = 0.1$ Oe at the frequency 1 kHz. In the process of measurements, the number of Metglas layers N was reduced from 12 to 3. The results of measurement are given in Fig. 12a. The measurement of the charge ME coefficient depending on the frequency for the optimal number ($N = 5$) of Metglas layers when applying the optimal constant MF is given in Fig. 12b.

In quasistatic measurements, the ME coefficient was 61.5 V/(cm Oe) with the number of Metglas layers $N = 5$ and optimal value of the constant field $H_{dc} = 5$ Oe. Dynamic measurements of the charge ME coefficient (α_Q) demonstrate the maximal value at the frequency of longitudinal electromechanical resonance of the structure $f = 25$ kHz. The maximal value is $\alpha_Q = 80$ nC/Oe, which corresponds to the ME coefficient in terms of voltage $\alpha_E = \alpha_Q/(Ct) = 1280$ V/(cm Oe), where $C = 3120$ pF (capacity of the piezoelectric material) and $t = 0.02$ cm (thickness of the piezoelectric layer).

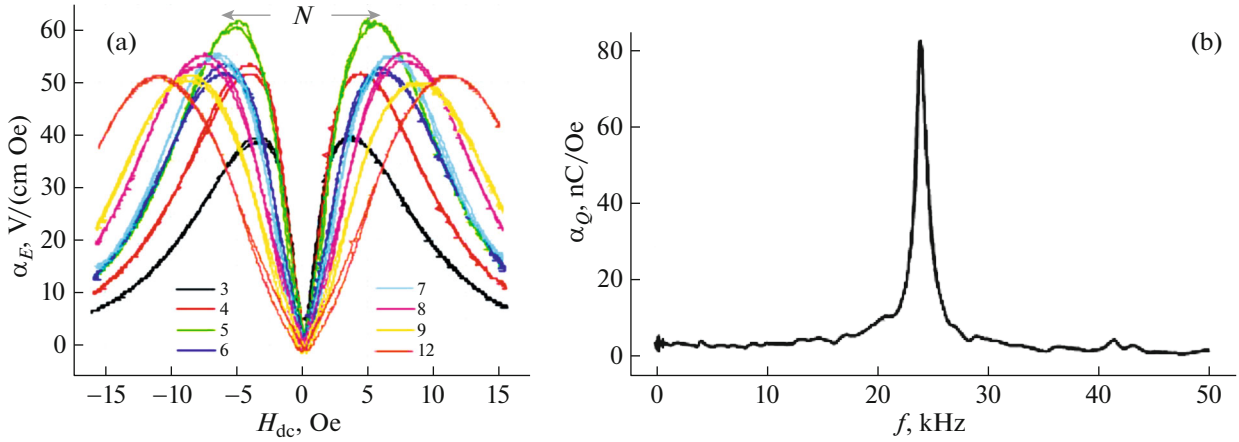

Fig. 12. ME coefficient as a function of the constant MF for the structure Metglas/PMN-PT doped with Mn with different numbers N of Metglas layers (a). Charge ME coefficient depending on the frequency of a variable MF (H_{ac} = 0.05 Oe) when applying the optimal constant MF H_{dc} = 5 Oe for N = 5 (b) [92] (graphs copied with permission of AIP Publishing © 2021).

In most works, lead-containing ferroelectric materials (PZT, PMN-PT, PZN-PT) are used to create composite multiferroics. However, they have a number of disadvantages: a low Curie temperature, nonlinear dependence of the properties on the temperature, significant mechanical-electrical hysteresis, and parasitic pyroelectric effect [93]. In [93], it was proposed to measure the ME effect in composite structures based on lead-free piezoelectric crystals of langatate (LGT, $Ca_3Ga_2Ge_4O_{14}$) of a x-cut and to compare with PZT (#APC85) and PMN-PT [001]. Three-layer samples with the $L-T$ structure were studied in the work (Fig. 7b). Permendur (Fe–Co–V alloy), which has a large value of magnetostriction $\lambda \approx 70$ ppm (at $H_{dc} \approx$ 100 Oe), was used as a magnetostrictive layer. Triple structures P–LGT–P, P–PZT–P, and P–PMN-PT–P were prepared by gluing layers of permendur with a piezoelectric crystal with epoxy glue. The sizes of the LGT piezocrystal and PZT piezoceramic were the same (25 × 4.5 × 0.4 mm). The PMN-PT piezoceramic was slightly shorter and had a size 20 × 4.5 × 0.3 mm. The permendur layers had the same length and width as the piezoelectric layer; the thickness was 0.16 mm. The quasistatic ME coefficient depending on the applied constant MF (Fig. 13a) and dynamic ME coefficient depending on the frequency of MF modulation (Fig. 13b) were measured.

The ME coefficient is directly proportional to the ratio of the transverse piezoelectric coefficient to the dielectric permeability of the material (d/ε). For LGT, d_{11}/ε_{11} = 0.25 pm/V; for PZT, d_{13}/ε_{33} = 0.1 pm/V; and for PMN-PT, d_{13}/ε_{33} = 0.15 pm/V. This ratio indicates that the ME coefficient must be larger in the structure based on LGT. Indeed, the largest ME coefficient in the quasistatic measurements was demonstrated by the sample based on P–LGT–P (α_E = 6.3 V/(cm Oe)), then by the sample P–PMN-PT–P (α_E = 1.4 V/(cm Oe)), and the lowest ME effect was demonstrated by the sample P–PZT–P (α_E = 0.6 V/(cm Oe)). At the resonance frequency, the P–LGT–P sample also demonstrated the largest ME coefficient (α_E = 155 V/(cm Oe)), while the P–PMN-PT–P structure demonstrated the minimal ME effect (α_E = 70 V/(cm Oe)). Thus, lead-free piezoelectric materials with low values of the piezoelectric coefficient can be useful in ME composite structures and demonstrate results that are superior to composite multiferroics based on widely used lead-containing ferroelectrics.

In [18], a study of the ME effect was carried out in the composite samples based on LN crystals as compared with the structure based on a PMN-PT crystal. Ferroelectric LN crystals have a number of advantages: relatively low cost, high chemical and temperature stability, absence of creep and mechanical-electrical hysteresis, and a high Curie temperature (1140°C). Moreover, they are produced by industry in large volumes and have excellent reproducibility of their properties. LN crystals with the y + 41°-cut and y, as well as the PMN-PT (011) cut polarized parallel to the direction 011 (along the sample thickness), were suggested in the work as the piezoelectric phase. All samples were square in shape and had a size of 10 × 10 × 0.5 mm. Metglas with a thickness of 29 μm was used as the magnetostrictive layer. Three-layer samples with the $L-T$ structure (Fig. 14c) were prepared via gluing with epoxy glue. Measurements of the ME coefficient were carried out for two directions (x and y) in the sample plane. Measurements in different directions are required due to the anisotropy of the piezoelectric effect in LN and PMN-PT crystals. In the PMN-PT crystal, the piezoelectric coefficient is d_{31} = –1700 pm/V when stretched along the direction x and d_{32} = 850 pm/V in the direction y. The dielectric permeability ε_{33} (along the sample thickness) mea-

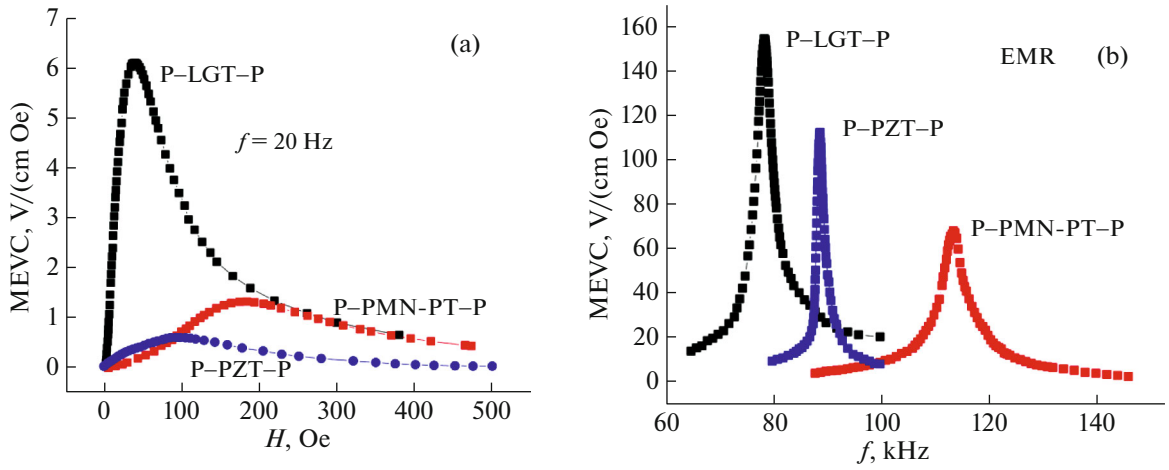

Fig. 13. Dependence of the ME coefficient on a constant MF at a frequency of the modulating field of 20 Hz and amplitude of H_{ac} = 1 Oe (a). The ME coefficient depending on the frequency of the variable MF (H_{ac} = 1 Oe) when applying the optimal constant MF (b). The maximal values of the ME coefficient correspond to the longitudinal electromechanical resonance of the structures [93] (graphs copied with permission of AIP Publishing © 2021).

sured at the frequency f = 1 kHz is 4440. For LN crystals of the y + 41°-cut and y-cut, the piezoelectric coefficients are d_{31} = –16 pm/V and d_{32} = –17.5 pm/V, d_{31} = –20.8 pm/V, and d_{32} = 0 pm/V, respectively. The dielectric permeabilities ε_{33} of these crystals are 45 and 69 for the y + 41°-cut and y-cut, respectively. Thus, it can be expected that the ME coefficient in a certain direction will be larger than in others.

The ME coefficient was measured in two modes: the quasistatic α_{E3i} (depending on the constant MF) and dynamic (α_{E31} depending on the frequency of the MF) modes. The amplitude of the variable MF was H_{ac} = 1 Oe. The quasistatic measurements were carried out at a frequency of 5 kHz. The results of the measurements are presented in Fig. 14 [18].

A three-layer composite structure on the basis of an LN crystal of the y-cut has in the quasistatic case (Fig. 14a) a ME coefficient of α_{E31} = 0.46 V/(cm Oe) when the MF is directed along the axis x, while it has a value of α_{E32} = –0.024 V/(cm Oe) when the MF is directed along the axis y, which magnitude is less by an order. In an ideal case, the value α_{E32} must be zero due to the zero value of the piezoelectric coefficient in the direction y; however, there are parasitic signals in the experiment in the form of Faraday's electromagnetic induction and other adjustments on the measuring system, which leads to the emergence of a nonzero signal. A correction for the measured ME coefficient for this value is given in the work. For the structure based on a PMN-PT crystal, the ME coefficient is α_{E31} = 1.15 V/(cm Oe), which corresponds to the direction of the largest piezoelectric effect (d_{31}), when the ME coefficient α_{E32} = –0.41 V/(cm Oe) is more than 2 times less. On the other hand, the isotropic behavior of the ME coefficient for these two directions (x and y) $\alpha_{E31} \approx \alpha_{E32}$ = 0.42 V/(cm Oe) is observed for the composite multiferroic based on LN of the y + 41°-cut. Thus, by choosing the right cut of the crystal, the ME properties of three-layer composite multiferroics can be changed quite a lot. We note that the optimal MF (corresponding to the maximal value of α_{E3i}) in the quasistatic mode of measurements was ~25 Oe for all three structures. The structure based on PMN-PT demonstrated a ME coefficient 3 times larger than that based on LN crystals.

According to the results of measurements of the dependence of the ME coefficient on the frequency of a MF, it was found that composite multiferroics on the basis of LN at the frequency of longitudinal electromechanical resonance can have a larger ME response than the structures based on PMN-PT (Fig. 14b). For a three-layer structure on the basis of LN of y + 41°-cut, the ME coefficient was 90 V/(cm Oe), while it was only 70 V/(cm Oe) for PMN-PT at the resonance frequency. Thus, three-layer composite multiferroics on the bases of LN crystals can be used as an alternative to ME structures on the basis of lead-containing piezoelectrics.

Thin-film samples, in which functional layers of piezoelectric and magnetostrictive materials are sputtered onto a silicon substrate by the target magnetron sputtering method, became another interesting direction in the development of composite ME materials [82, 94, 95]. AlN is used as the piezoelectric material. Metglas ($Fe_{70.2}Co_{7.8}Si_{12}B_{10}$) is the magnetostrictive material. The layered scheme of this composite material is presented in Fig. 15a. Single-sided support of the structure allows one to observe a low-frequency bending resonance, at which amplification of the ME signal occurs. Such a design is attractive for highly sensitive MF sensors at low frequencies. In [82], in

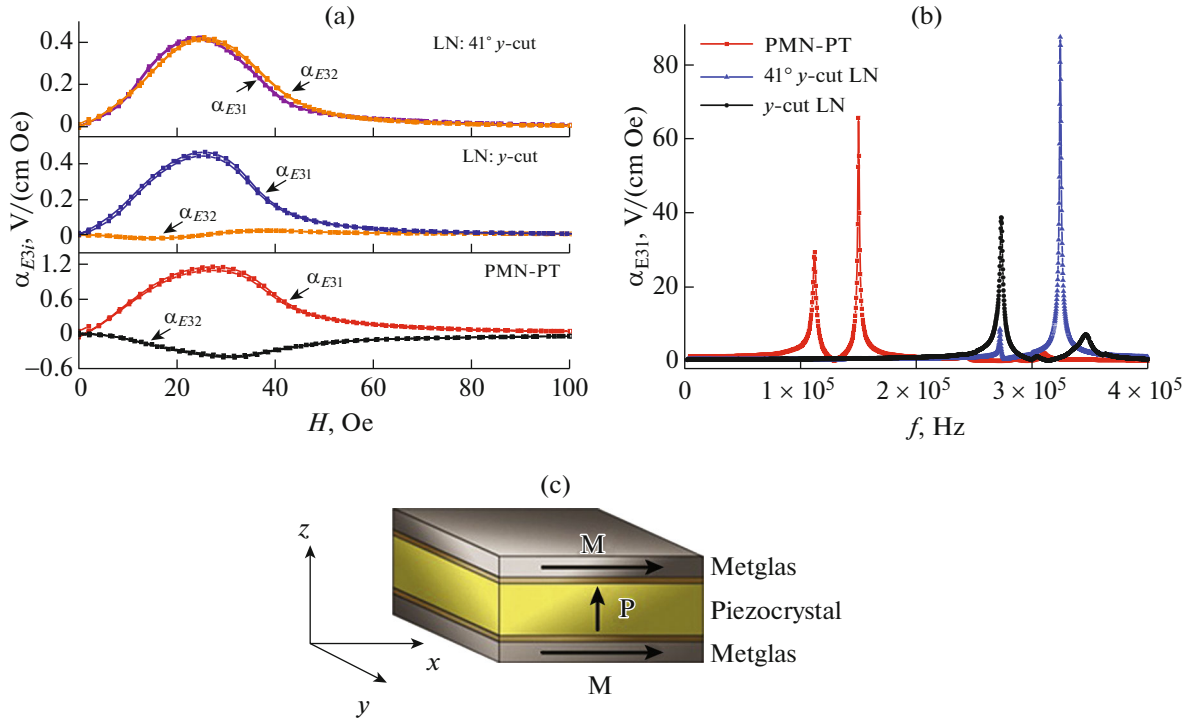

Fig. 14. Quasistatic measurements of the direct ME coefficient depending on the value of the constant MF along the directions x and y in the structures Metglas/piezoelectric/Metglas (a). Dynamic measurements of the ME coefficient depending on the frequency of the MF with applied optimal constant MF $H_{dc} = 30$ Oe (b). Schematic image of three-layer $L-T$ structure with axis directions and electrode designation (c) [18] (graphs and figure copied with permission of AIP Publishing © 2021).

order to increase the ME coefficient and decrease the frequency of bending resonance, a groove with a size of 7 mm in length, 4 mm in width, and 0.65 mm in depth was etched into a silicon substrate; thus, the silicon substrate was thinned to 90 μm. The total width of the structure was 4 mm. The thicknesses of the AlN piezoelectric layer and Metglas magnetostrictive layer were 2 μm. AlN was selected due to its high ratio $d/\varepsilon = 0.23$ pm/V. The piezoelectric coefficient $d_{31} = -2$ pm/V and $\varepsilon_{33} = 8.5$ [22, 96, 97].

In [82], measurements of the ME coefficient were performed depending on the frequency of the modulating MF when applying the optimal constant MF (6 Oe). The results of measurements of the ME coefficient depending on the pressure of the surrounding atmosphere were also presented. The experimental results are presented in Fig. 15b.

The ME coefficient at the resonance frequency 167.85 Hz was 9 kV/(cm Oe) under atmospheric pressure. At a pressure of 3×10^{-5} bar, the ME coefficient increases to a record value of 19 kV/(cm Oe), which indicates that friction against air even at a low frequency of 167 Hz contributes greatly to a reduction in the useful signal from the ME structure. This experimental result can be subsequently used when producing sensors, creating a forevacuum when the device is packaged.

We note that when calculating α_E, it is necessary to carry out normalization to the sample thickness; in this case, the piezoelectric material is an AlN film with a thickness of only 2 μm, although it is applied to a substrate with a thickness of 740 μm; therefore, it will be fair to compare the result obtained with others, multiplying α_E by the thickness of the piezoelectric layer ($\alpha_t = \alpha_E t$). Then the ME coefficient is $\alpha_t = 3.8$ V/Oe, which is comparable or even less than in the above works. The coefficient α_t is also used to calculate the limiting sensitivity of ME material to a MF, which is important for the use of composite multiferroics in sensors of ultra-weak MFs.

The main parameters of the composite multiferroics considered above are given in Table 2.

Analysis of the mentioned works demonstrates that the quasistatic ME coefficient is larger in structures based on lead-containing crystals PZT or PMN-PT and PZN-PT than in the samples based on lead-free crystals. However, this is due to the larger thickness of magnetostrictive phase. In [18, 93], a comparison was made under equal conditions, when the thickness of the magnetostrictive layers was the same. In this case, structures based on lead-free piezoelectric crystals demonstrated values of the ME coefficient that were either comparable or several times larger. However, it is necessary to use theoretically predicted values of the

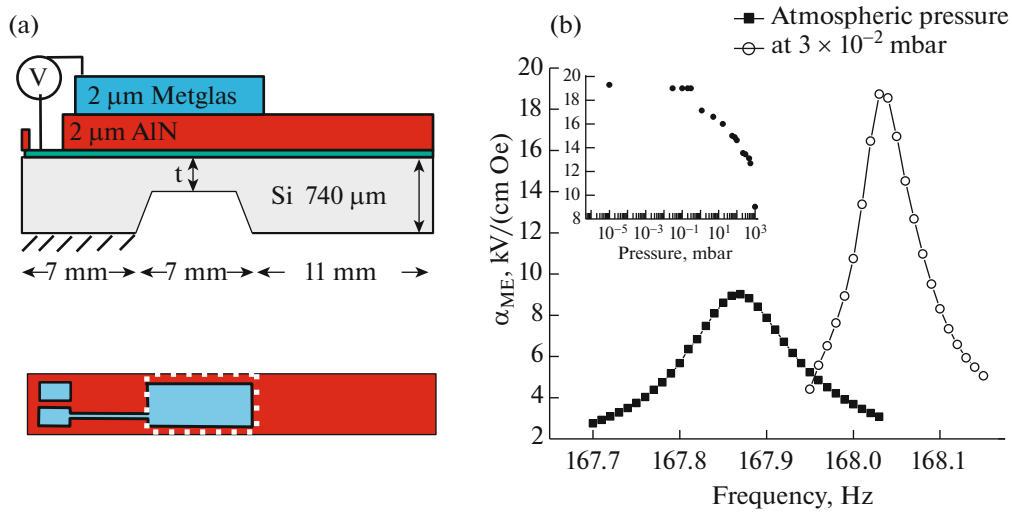

Fig. 15. Schematic image of the ME structure (a). ME coefficient close to the resonance frequency (167.85 Hz) at atmospheric pressure and in vacuum (b). The dependence of the ME coefficient at the resonance frequency on the air pressure is presented in the insert [82] (figure and graph copied with permission of John Wiley and Sons © 2022).

ratio of the thicknesses of the piezoelectric and magnetostrictive layers for each of the materials for correct comparison.

In the case of measurement of the dynamic ME coefficient, the samples containing piezoelectric crystals on the basis of LGT and LN demonstrated larger values of the ME effect than structures on the basis of lead-containing PZT or PMN-PT crystals.

From the point of view of the application of composite multiferroics in MF sensors, the temperature stability of the piezoelectric and mechanical properties of the piezoelectric material, absence of nonlinearity, hysteresis, and creep during deformation, and relatively low cost of production play a significant role. The listed requirements are met by lead-free LN crystals. This material has great potential for applications in ME structures and devices on their basis.

3. BIMORPH COMPOSITE ME STRUCTURES

High values of the ME coefficient in composite multiferroics open up a way to create highly sensitive MF sensors and current sensors that can potentially be passive (do not require an additional electrical supply). In this regard, the limiting sensitivity to a constant or variable MF, which is determined by the external and internal noise of the ME composite, is a very important parameter for ME structures. The internal noise is determined by thermal noise (Johnson–Nyquist noise). However, external noise excited from

Table 2. Main results of measurements of the ME coefficient for the considered structures

Samples	$\|d/\varepsilon\|$, pm/V	Dynamic ME coefficients α_E (V/(cm Oe)) and α_t (V/Oe)	Resonance frequency, kHz	Quasistatic ME coefficient, V/(cm Oe)
Piezo fiber (PZT)/Metglas (L—L) [89]	0.33 [98]	470, 4.7	10.5	23
FeBSiC/PZN-PT (L–T) [91]	0.51	400, 4	20	10
Metglas/PMN-PT, Mn-doped (L—T) [92]	1.38	1280, 25.6	25	61.5
Permendur/LGT/ Permendur (L—T) [93]	0.25	155, 6.2	80	6.3
Permendur/PZT/ Permendur (L—T) [93]	0.1	110, 4.4	90	1.4
Permendur/PMN-PT/ Permendur (L—T) [93]	0.15	70, 2.1	110	0.6
y + 41°-cut LN/Metglas (L—T) [18]	0.39	90, 4.5	330	0.4
y-cut LN/Metglas (L—T) [18]	0.3	40, 2	270	0.4
(011)-cut PMN-PT/Metglas (L—T) [18]	0.38	70, 3.5	150	1.2
AlN/Metglas on silicon substrate (L—T) [82]	0.23	9000, 1.8	0.167	–

Sample structure, $|d/\varepsilon|$ ratio, values of the dynamic and quasistatic ME coefficients, and resonance frequency of the structures are given.

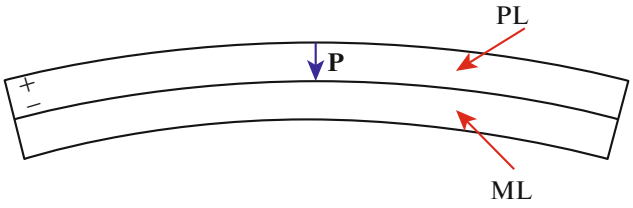

Fig. 16. Schematic illustration of the effect of thermal and vibration noise on the ME structure on the basis of a unimorph structure (ML ia the magnetostrictive material; PL is the piezoelectric material; **P** is the polarization vector; "+" and "–" are the signs of the charges formed on the surface of the piezoelectric material due to parasitic vibrations and temperature fluctuations) [17] (figure copied with permission of AIP Publishing © 2021).

the environment (for example, thermal fluctuations, mechanical vibrations, and electromagnetic interference) makes the greatest contribution in practice [17]. The pyroelectric effect introduces additional noise. Vibration noise has a piezoelectric origin. Therefore, it is necessary to look for ways to reduce the effect of this noise on the useful ME signal in composite multiferroics.

In [17], the ability of different configurations of ME structures to suppress both vibration noise and external thermal fluctuations (external thermal noise) was demonstrated. Vibration noise causes two types of deformations in composite structures, including stretching (compression) and bending deformations. The bending deformations make the largest contribution due to their low frequency, since vibration noise in the environment most often has a low-frequency nature. Such noise can be suppressed using mechanically symmetrical structures. Thermal noise will cause stretching (compression) deformation and bending deformation of the material.

The scheme of a ME structure consisting of piezoelectric and magnetostrictive materials of different thicknesses is presented in Fig. 16. The demonstrated unimorph configuration is nonsymmetrical. Therefore, it will be impossible to separate the vibration noise and useful ME signal. In a similar way, external thermal noise cannot be suppressed in this structure.

In the case when the thickness of the magnetostrictive layer is much less than the thickness of the piezoelectric with a unimorph structure, bending fluctuation modes will be suppressed due to the compensation of charges on the surface of the piezoelectric; thus, the vibration noise will be completely compensated. However, no amplification of the ME effect at the frequency of the bending resonance will also be observed. Similar arguments can also be given for thermal noise.

The scheme of a ME sample on the basis of a bimorph piezoelectric material is given in Fig. 17. The thicknesses of the piezoelectric and magnetostrictive materials are equal. Such a structure is nonsymmetrical. Longitudinal fluctuation modes in this design will be suppressed due to the bimorph structure of the piezoelectric. Therefore, vibrations inducing the bending fluctuation mode of the sample will make the largest contribution to the noise. However, partial compensation of the vibration noise will be observed in this structure due to the location of the neutral plane (that plane in the material not experiencing deformation) at the boundary between the piezoelectric and magnetostrictive material. Both bending and longitudinal deformations of the structure can arise when thermal fluctuations affect the material. An illustration of the above-described effects on the structure is presented in Fig. 17.

The parasitic signal is completely suppressed during the effect of thermal noise in the case of longitudinal fluctuations. With bending fluctuations, there is partial compensation of the thermal noise due to the fact that the neutral plane is located at the boundary between the piezoelectric and magnetostrictive material; therefore, charges formed at the edges of the piezoelectric are not completely compensated [17, 30]. At the same time, the ME signal will also be compensated partially. The greater the distance from the neutral plane to the piezoelectric bimorph, the less useful the signal will be. In the case when the thickness of the magnetostrictive layer is much less than the thickness of the bimorph, the neutral plane is located in the middle of the piezoelectric material. In this case, the thermal noise will be completely suppressed, while vibrations inducing the bending-deformation mode will be intensified in the same way as the useful ME signal. The structure, in which there are two magnetostrictive layers of the same thickness (between which the bimorph is located), will work in a similar way (Fig. 18).

The direction of magnetization in the magnetostrictive materials is opposite to each other. In such a case, the ME effect will be increased due to an increase in the thickness of the magnetostrictive layer.

We also consider another bimorph ME structure with symmetrical location of the magnetostrictive layers (Fig. 19). A bimorph piezoelectric layer consists of two crystals (PL 1 and PL 2) with oppositely directed vectors of polarization. The contacts between the upper edge of the PL 1 crystal and lower edge of the PL 2 crystal are connected to each other. In the place where there is a connection between the PL 1 and PL 2 crystals, there is a second contact, which is grounded in the experiment. The plane between the crystals PL 1 and PL 2 is neutral. When the vibration noise affects such a structure, it will experience bending deformation. As a result, charges of different sign and different value will be formed on the upper and lower edges of the piezoelectric sample, which will lead to their compensation.

However, such a design will also suppress the ME signal at the frequency of bending resonance. This leads to the fact that the structure is an analogue of the above considered unimorph one, in which the thickness of the magnetostrictive layer is much less than the thickness of the piezoelectric.

For most of the structures presented in [17], measurements of the signal–noise ratio (SNR) depending on the frequency were carried out (Fig. 20). These measurements demonstrated the sensitivity of each of the structures to variable MF under the influence of the same vibration signal.

Based on the data presented in Fig. 20, it can be concluded that the samples with a symmetrical bimorph ME structure (LT–PP), ME samples with a symmetrical structure based on unimorph piezoelectric material (LT), and asymmetrical bimorph ME samples (Bimorph) have the greatest sensitivity to MF. The samples with an asymmetrical ME structure based on a unimorph piezoelectric have the lowest sensitivity.

An increase in the sensitivity to MF in the low-frequency region (1–200 Hz) for the LT–PP and LT samples is associated with suppression of the signal, which occurs at bending fluctuations of the structure. However, it will be impossible to obtain amplification of the ME signal at bending low-frequency electromechanical resonance. Asymmetrical bimorph ME structures are able to suppress partially both the vibration noise and noise caused by the pyroelectric effect. Such a design will enhance the ME effect at the frequency of bending resonance; however, low-frequency vibration noise will also be amplified.

Measurements of the piezoelectric signal and limiting sensitivity to low-frequency MF as compared with an asymmetrical unimorph ME sample were carried out for bimorph ME structure in [30]. The structure and linear sizes of the bimorph ME sample are presented in Fig. 21a. The linear sizes and magnetostrictive-layer material in the unimorph ME sample are the same as in the bimorph sample.

When measuring the dependence of the pyroelectric signal on the temperature in the bimorph ME, the pyroelectric current decreases more than 10 times as compared with the single-domain ME sample (Fig. 21b).

Measurements of the limiting sensitivity of the ME samples to the magnetic field in a low-frequency spectral region (10^{-1}–10 Hz) were carried out. The measurements of the magnetic-noise density for the bimorph and single-domain ME samples are presented in Fig. 22.

The limit of the sensitivity to a MF for a bimorph sample is 20 pT/Hz$^{1/2}$ at a frequency of 1 Hz. At the same time, the single-domain sample demonstrated the sensitivity 1 nT/Hz$^{1/2}$ at a frequency of 1 Hz. The result obtained demonstrates a potential for reduction of the equivalent noise due to a decrease in the contribution of the pyroelectric signal.

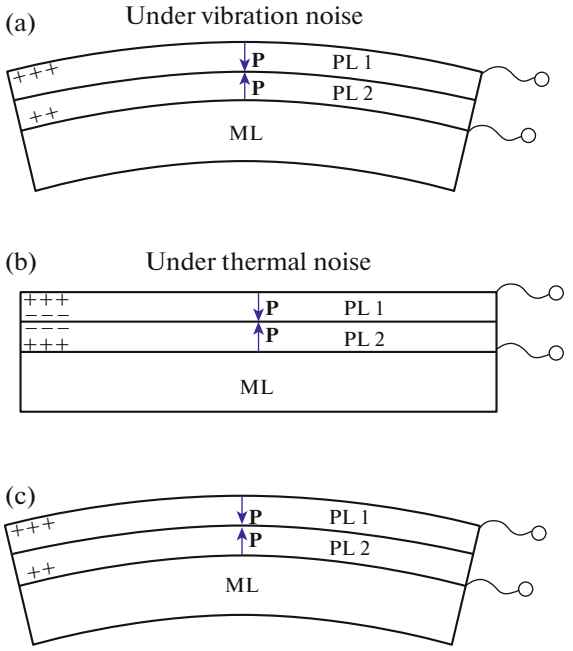

Fig. 17. Effect of environmental noise on the bimorph ME sample: (a) vibration noise exciting bending vibrations of the structure, (b) thermal noise exciting longitudinal vibrations of the structure, and (c) thermal noise exciting bending vibrations of the structure [17] (figures copied with permission of AIP Publishing © 2021).

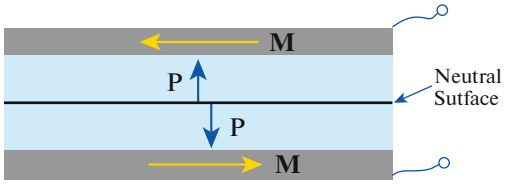

Fig. 18. ME structure with a bimorph piezoelectric and two symmetrically located magnetostrictive layers.

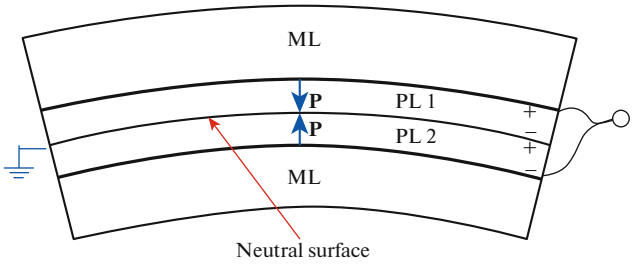

Fig. 19. Schematic image of the symmetrical bimorph ME structure (LT–PP) [17] (figure copied with permission of AIP Publishing © 2021).

The bimorph ME structure presented in Fig. 21a is able to suppress efficiently the pyroelectric noise, as well as to decrease partially the external vibration noise.

The main conclusions on the above given designs of ME structures are as follows: it is impossible to sup-

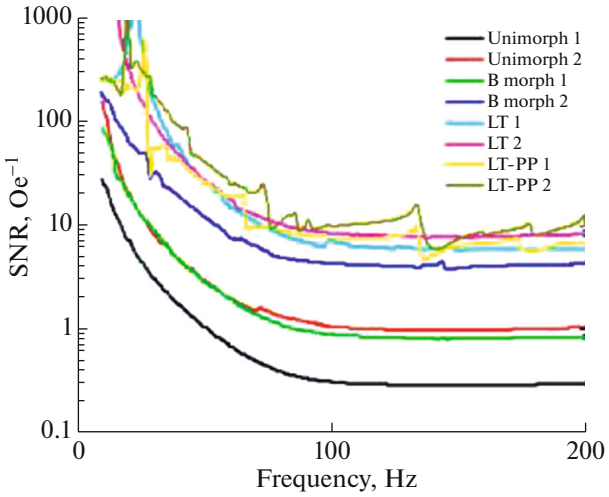

Fig. 20. Signal-to-noise ratio for different types of ME structures [17] (graphs copied with permission of AIP Publishing © 2021).

press simultaneously thermal and vibration noise within the same design, thus not excluding the signal from the bending-deformation mode; it is necessary to use the advantages of asymmetrical structures, where it is possible to separate the signal caused by the noise from a useful ME signal, to achieve the maximal sensitivity of ME structures to a magnetic field.

4. MEASUREMENT OF VARIABLE ULTRA-WEAK MAGNETIC FIELDS USING COMPOSITE MULTIFERROICS

The creation of highly sensitive sensors of ultra-weak MFs based on ME-composite multiferroics is one of the directions of use that is most promising and close to practical implementation [10–12]. The lack of a necessity to cool such sensors is a significant technical advantage over SQUIDs used now for these purposes without an alternative. It is obvious that MF sensors based on composite multiferroics cannot completely replace SQUIDs, which are capable of detecting individual quanta of a magnetic flux [13]; however, there are a number of applications, in which the use of MF sensors based on composite multiferroics is justified. Such areas of application include highly sensitive miniature magnetometers of industrial and research classes for the contactless measurement of ultra-weak currents, MFs in living organisms applied to magnetocardiography and magnetoencephalography, the visualization of magnetic nanoparticles, measurement of magnetic anomalies, magnetic geological exploration, etc.

Magnetocardiography, magnetoneurography, magnetoencephalography, and magnetomyography allow the efficient diagnosis and observation of diseases of different genesis, and local, as well as volume measurements (organ mapping) of MFs from studied objects to be carried out. It is important to note that the detection of biomagnetic signals makes it possible to obtain unreferenced and coherent measurements that do not depend on the dielectric properties of biological systems. These techniques are also able to effectively complement invasive studies (for example, deep stimulation of the brain by electrical signals). Magnetocardiography also makes it possible to obtain earlier information about cardiac fibrillation during human fetal development [99].

The listed methods require a high sensitivity to MFs at low frequencies. Therefore, the search and development of simple, cheap, miniature, and highly sensitive magnetic sensors (that can work at room temperature) is an important task of modern electronics and medicine. However, at the moment there is no sensor, which would satisfy all the above listed characteristics; therefore, the study of magnetic signals from human organs and tissues is insufficiently developed at present. In [99], there is a review of the most suitable magnetic sensors that can be used as an alternative to

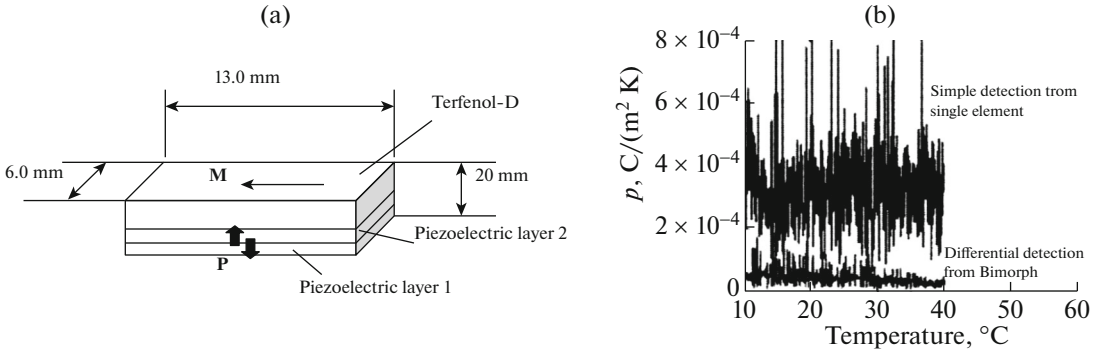

Fig. 21. Schematic image of the bimorph ME sample consisting of two identical piezoelectric PZT plates with opposite polarization ("tail-to-tail") and magnetostrictive material Trifenal D ($Tb_{0.27}Dy_{0.73}Fe_2$) (a). Measurement of the pyroelectric signal depending on the temperature for bimorph ME and unimorph ME samples (b) [30] (figure and graph copied with permission of AIP Publishing © 2021).

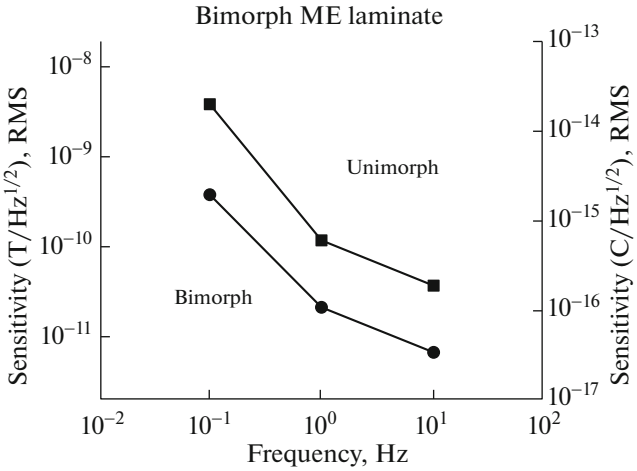

Fig. 22. Density of the magnetic noise for ME samples with different domain structure of the piezoelectric layer (bimorph and unimorph) [30] (graph copied with permission of AIP Publishing © 2021).

a SQUID magnetometer. MF sensors suitable for biomedical applications include SQUID magnetometers, induction sensors, fluxmeters, magnetoelectric magnetometers, sensors based on the giant magnetoimpedance (GMI) effect, sensors based on the giant magnetoresistance (GMR) effect, optical pumping sensors, optomechanical sensors, Hall-effect sensors, magnetoelastic sensors, magnetometers based on spin wave interferometry, and sensors based on nitrogen-vacancy centers in diamond [99].

A diagram comparing the sensitivities of the listed magnetic sensors and methods for studying magnetic signals from human tissues and organs is presented in Fig. 23.

As follows from the diagram, SQUID magnetometers are able to accurately detect ultra-weak MFs at the level 1 fT/Hz$^{1/2}$. Optical pumping sensors, induction sensors, and magnetoelectric sensors can be an alternative to SQUID magnetometers. ME sensors have a number of advantages, including small linear sizes (a combination with MEMS technology is possible), low cost of production, ability to work at room temperature, passivity (do not consume electricity for signal detection). A dependence of the limiting sensitivity of the listed sensors to MFs on the signal frequency is demonstrated in Fig. 24 [100].

Useful magnetic signals from the human heart and brain have an amplitude from ranges of fT/Hz$^{1/2}$ to 100 pT/Hz$^{1/2}$ in the range of frequencies from mHz to 300 Hz, which is the most noisy low-frequency region [16, 100]. This leads to the need to use vibration- and magnetically protected spaces for the detection of such fields.

To date, sensors based on composite multiferroics are able to detect MFs on the order of units of pT/Hz$^{1/2}$; moreover, new works are regularly published, in which this threshold decreases due to the improvement of processing electronics and a change in the sensor design [10, 14, 15]. Such a sensitivity is sufficient for detecting MFs induced by currents of the α rhythm of the brain with amplitudes in units of pT (magnetoencephalography) and currents flowing in the human heart (magnetocardiography) [11, 16]. On the other hand, to study the activity of the cerebral cortex, it is necessary to measure with a high degree of reliability MFs that are 1–2 orders of magnitude

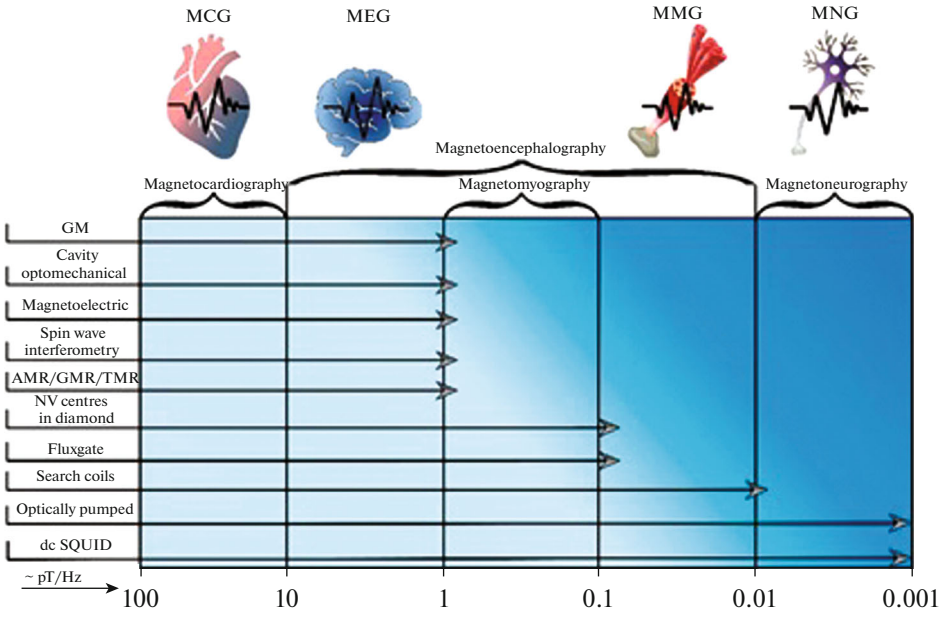

Fig. 23. Diagram comparing the sensitivities of different types of magnetic sensors (*y* axis) with the ability to detect different biomagnetic signals (*x* axis) [99] (figure copied and adopted in accordance with the license CC BY 4.0).

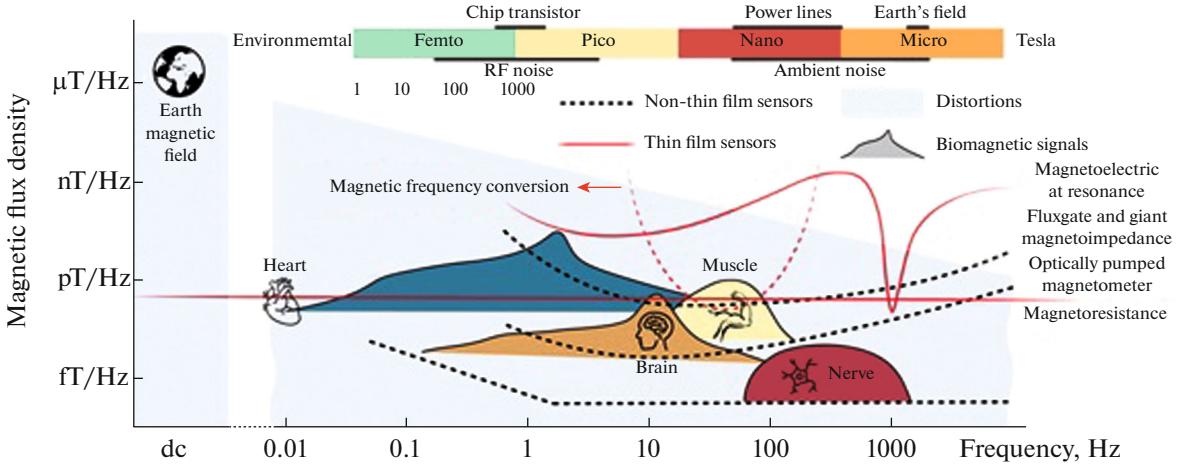

Fig. 24. Comparison of the values of the limiting sensitivity of sensors to MFs required for signal detection from different biological systems. The external noise level is shown in gray [100] (figure copied in accordance with the license CC BY 4.0).

lower. At the moment, such a level of sensitivity of a sensor based on a composite multiferroic has not been realized by any research team around the world.

The sensitivity of a ME sensor is mainly limited by its own noise, in which thermal Nyquist noise and 1/f noise dominate [2, 17]. Thermal noise can be minimized due to the use of appropriate schemes for detecting a weak output signal from ME structures [21]. Suitably designed schemes of detection based on voltage or charge amplifiers should have a noise amplitude at the level of the limit of sensitivity of these components [22, 23]. On the other hand, external noise caused by piezoelectric vibrations, pyroelectric noise, and magnetic sources of noise require more complex strategies to deal with them [10, 24, 25].

It is known that asymmetrical two-layer systems containing a mechanical-electrical transducer of the bimorph type demonstrate especially large ME coefficients at bending resonance [26–29]. At the same time, to increase significantly the ME effect at low frequencies, the bimorph can be fastened in the form of a cantilever [10]. In addition to an increase in the sensitivity at low frequencies and an increase in the ME coefficient, such a design is able to compensate partially the vibration and thermal noise [17, 30].

We consider the effect of the thermal noise of a ME structure and input noise of the detection scheme (preamplifier) on the value of the limiting sensitivity of a ME sensor to a variable MF, following the arguments given in the work [22], in which an analysis of the indicated noise was carried out for a ME sample on the basis of AlN/Metglas composite material connected to an operational amplifier.

The ME sensor consists of a silicon cantilever, to which functional layers of aluminum nitride and Metglas were sputtered. The sensor was glued with epoxy glue to the holder.

The thermal noise associated with the final resistance of the piezoelectric phase and described by E_{ME} voltage is the main source of intrinsic noise in ME composites:

$$E_{\mathrm{ME}} = \sqrt{4k_{\mathrm{B}}T\Delta f R_{\mathrm{ME}}}, \qquad (6)$$

where $k_{\mathrm{B}} = 1.38 \times 10^{-23}$ J/K is the Boltzmann constant; T is the temperature in K; Δf is the signal bandwidth in Hz; and R_{ME} is the equivalent resistance of the piezoelectric phase in Ω.

The thermal noise is caused by chaotic fluctuations of thermally excited charge carriers in a piezoelectric. Metglas has a low resistance, which allows us to ignore the thermal noise in this layer.

The thermal-noise voltage normalized to the sensor output depends on the capacity (C_{ME}) of the ME sample [22]:

$$E'_{\mathrm{ME}} = \frac{E_{\mathrm{ME}}}{\sqrt{1 + (\omega C_{\mathrm{ME}} R_{\mathrm{ME}})^2}}. \qquad (7)$$

As follows from the expression (7), in order to keep the thermal-noise voltage low, we need to have the largest possible sample capacity.

The input noise current and noise voltage of the operational amplifier (I_n and E_n), as well as the thermal noise of the feedback resistance (R_j), are another source of noise. The feedback resistance creates the thermal noise $E_j = \sqrt{4k_{\mathrm{B}}TR_j}$.

The total noise reduced to the output of the operational amplifier E_{ov} is as follows:

$$E_{ov}^2 = E_{ovEn}^2 + E_{ovIn}^2 + E_{ovE1}^2 + E_{ovE2}^2 + E_{ov\mathrm{ME}}^2, \qquad (8)$$

where $E_{ovEn}^2 = G_v^2 E_n^2$, $E_{ovIn}^2 = (|Z_{\mathrm{ME}}|G_v^2 + R_2^2)I_n^2$, $E_{ovE1}^2 = (G_v - 1)^2 E_1^2$, $E_{ovE2}^2 = E_2^2$, and $E_{ov\mathrm{ME}}^2 = G_v^2 \dfrac{1}{1 + (\omega C_{\mathrm{ME}} R_{\mathrm{ME}})^2} E_{\mathrm{ME}}^2$. G_v is the operational-amplifier amplification coefficient.

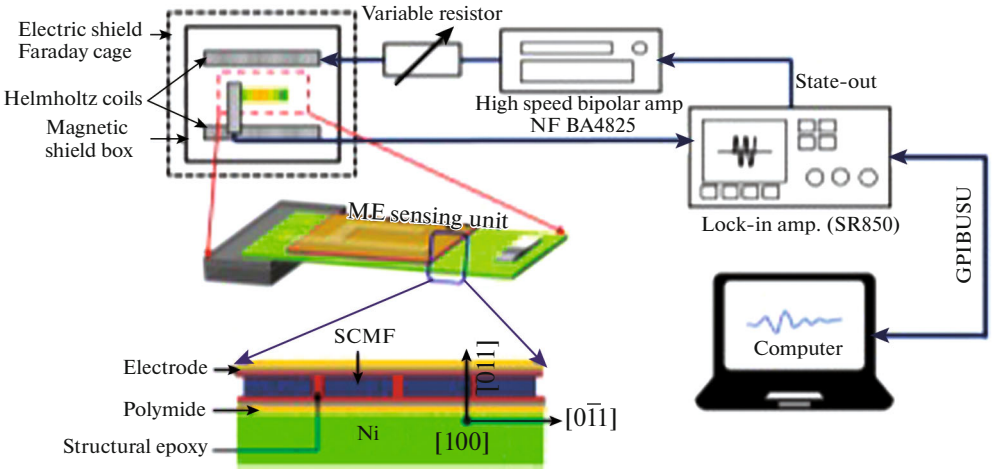

Fig. 25. Scheme of a device for measuring the sensitivity of a ME sensor and layered scheme of the structure [15] (image copied with permission of Elsevier © 2021).

In the work, the total noise was calculated at the output of the operational amplifier AD745.

The current noise of the operational amplifier (I_n) is a dominating noise at low frequencies; therefore, it is necessary to select operational amplifiers with the lowest value of input current noise for measurement at a low frequency.

The noise of the ME sensor and operational amplifier was measured at room temperature using a synchronous detector (SR785, Stanford Research Systems). The measurements were carried out in a magnetically protected chamber.

The sensitivity (S_i) of the composite structure at the resonance frequency 330 Hz will be equal to the noise of the entire detection system:

$$S_i = \frac{E_{ov}}{G_v \alpha_{ME} t} = \frac{11.66 \times 10^{-9}}{1200 \times 1.75} \frac{\text{T}}{\sqrt{\text{Hz}}} \approx 5.4 \frac{\text{pT}}{\sqrt{\text{Hz}}}. \quad (9)$$

Thus, external vibrations and electromagnetic interference create the most noise among many parameters that affect the final value of the sensitivity of ME sensors to low frequency MFs.

We consider the ways to reduce the influence of these parasitic signals on sensor operation and methods for increasing the sensitivity of ME structures to low frequency MFs.

In [15], it was demonstrated that a change in the dielectric-loss tangent in the piezoelectric material significantly increases the sensitivity of composite ME structures to MFs. The studied ME structure and the scheme of the measuring device are presented in Fig. 25.

The construction of the ME sensor consisted of a nickel plate ($55 \times 21 \times 0.25$ mm^3), onto which a piezoelectric layer (consisting of fibrous PMN-PZT material placed in an epoxy matrix) was glued with epoxy resin. Three crystals with different values of the dielectric-loss tangent were selected as the piezoelectric material: 40PMN-35PZ-25PT (with high losses, $\tan\delta = 0.0154$), 40PMN-35PZ-25PT with the addition of WO_3 at a concentration of 1 mole fraction (with average losses, $\tan\delta = 0.0098$), and 40PMN-35PZ-25PT with the addition of MnO at a concentration of 1 mole fraction (with low losses, $\tan\delta = 0.006$). The ME sensor was fastened in the form of a cantilever to decrease the resonance frequency of the structure, a permanent magnet with the weight 4.4 g (intended to form a constant displacement field on the magnetostrictive material and to decrease the bending resonance frequency) was fastened at the free end.

Measurements of the limiting sensitivity for each sample were carried out at the resonance frequency 500 Hz and a low frequency of 5 Hz. The results of the measurements are presented in Fig. 26.

At a frequency of 500 Hz, the maximal sensitivity of the ME sensors was 25, 500 pT and 5 nT for the composite structures on the basis of piezoelectric materials with low, medium, and large dielectric losses, respectively. The same dependence of a decrease in the sensitivity on an increase in the tangent of the dielectric-loss angle in the material is observed at the frequency 5 Hz. The maximal value of the limiting sensitivity to MFs is 120 pT at a frequency of 5 Hz for the sample with low dielectric losses. Thus, the use of piezoelectric materials with the minimal possible value of the tangent of the dielectric-loss angle is one of the ways to increase the sensitivity.

In [24], a frequency-conversion technique based on amplitude modulation of the magnetic signal to decrease the effect of low-frequency noise on useful-signal detection was proposed. The ME coefficient is proportional to the derivative of magnetostriction with respect to a change in the MF according to the formula (5). Magnetostriction has a quadratic dependence on the MF at low amplitudes. There is also a bending point, at which the curvature of the function

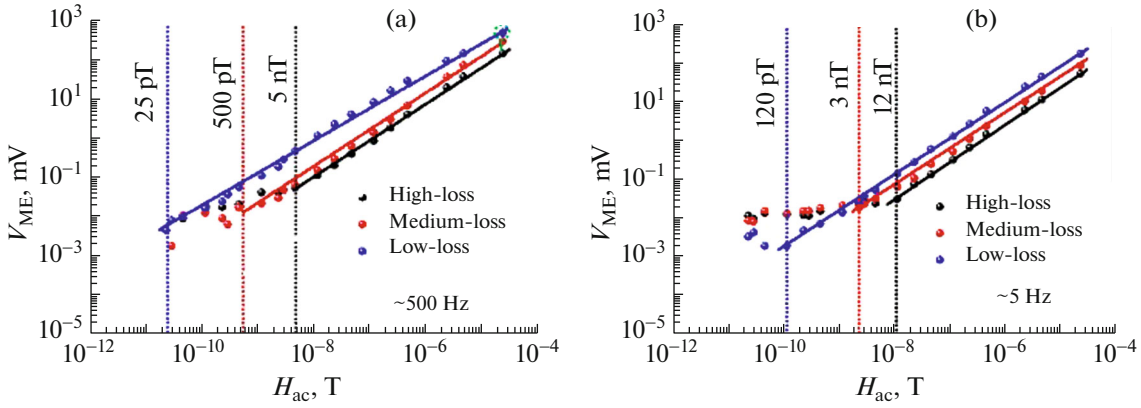

Fig. 26. Dependence of the output voltage applied to the ME sensor on the amplitude of the variable MF at the frequency 500 (a) and 5 Hz (b) [15] (graphs copied with permission of Elsevier © 2021).

of the dependence of magnetostriction on the MF changes from convex to concave. This point corresponds to the maximum of the ME-coefficient value depending on the constant MF applied to the sample; this point is also called the optimal value of the MF. If some modulating magnetic field B_{mod} with an amplitude equal to the value of the optimal MF is applied to the sample, the ME signal from the sample will be equal to the maximal value of the ME coefficient with the frequency ω_{mod}. If a weak low frequency MF B_{AC} (which needs to be measured) is simultaneously applied, the dependence of magnetostriction on the applied modulating magnetic field B_{mod} and low frequency field B_{AC} will be

$$\lambda(B_{\text{mod}}(t) + B_{AC}(t))|_{\omega_{\text{mod}} \pm \omega_{AC}} = A_1 \cos(\omega_{\text{mod}} t) \times \widehat{B_{AC}} \cos(\omega_{AC} t) = \frac{A_1 \widehat{B_{AC}}}{2} \times [\cos((\omega_{\text{mod}} + \omega_{AC})t) + \cos((\omega_{\text{mod}} - \omega_{AC})t)], \quad (10)$$

where $B_{\text{mod}}(t) = \widehat{B_{\text{mod}}} \cos(\omega_{\text{mod}} t)$, $B_{AC}(t) = \widehat{B_{AC}} \cos(\omega_{AC} t)$, $\widehat{B_{\text{mod}}}$ is the amplitude of the modulating signal, $\widehat{B_{AC}}$ is the amplitude of the low-frequency magnetic signal; t is time; and A_1 is the Fourier coefficient depending on $\widehat{B_{\text{mod}}}$.

Thus, if a frequency of modulation of the MF lower than the resonance frequency of the ME sensor by the value of the frequency of detected (unknown) signal (B_{AC}) is selected, then the frequency of this signal will be converted with an increase in the frequency up to resonance of the ME sensor ($\omega_{\text{res}} = \omega_{\text{mod}} + \omega_{AC}$). It becomes possible to measure an unknown low-frequency magnetic signal with a low amplitude.

To validate the model, a ME structure consisting of a silicon cantilever, onto which a film of molybdenum with a thickness equal to the lower electrode was sputtered, was created. A piezoelectric layer of aluminum nitride (AlN) was grown over the molybdenum, and Metglas was sputtered over the AlN. A schematic image of the structure is presented in Fig. 27a.

The ME-response spectrum of the sensor with applied modulating signal with an amplitude of $B_{\text{mod}} = 0.56$ mT and frequency of 668 Hz, as well as a low frequency signal of $B_{AC} = 1$ μT with the frequency 1 Hz, is presented in Fig. 27b. The modulating-field frequency is chosen so that $f_{\text{res}} = f_{\text{mod}} + f_{AC}$. The signal at the resonance frequency contains necessary information about the MF. Two measurements were carried out to compare the limiting sensitivity of the ME sensor at a signal frequency of 1 Hz. The first was carried out without the use of frequency-conversion techniques, when the optimal constant MF is applied to the ME sensor, and variable MF at a frequency of 1 Hz decreases with a small step from 10 μT to 10 pT. The results of such measurement are given in Fig. 27c. The minimal detectable signal at the frequency 1 Hz (obtained using direct measurement) is 1 μT/Hz$^{1/2}$. The second measurement was carried out using the frequency-conversion technique. The modulating MF with the amplitude $B_{\text{mod}} = 0.56$ mT and frequency 668 Hz and variable low-frequency signal were simultaneously applied to the sensor. The amplitude of the variable magnetic signal at the frequency 1 Hz consistently decreased from 10 μT to 10 pT. The useful signal was recorded at the frequency $f_{\text{res}} = f_{\text{mod}} + f_{AC} = 669$ Hz. The results of the measurement are presented in Fig. 27d. An increase in the sensitivity by 1000 times was obtained [24]. The limiting detectable signal was 1 nT. We note that this technique completely solves the problem of low-frequency vibration noise, which is not detected at the frequency of measurement due to the mechanical nature of the signal (magnetostrictive material is sensitive to the electromagnetic effect).

It was possible to improve significantly the sensitivity of the ME sensor using the signal-frequency-conversion technique in [101]. The limiting sensitivity of the ME structure was 20 pT at a frequency of 1 Hz.

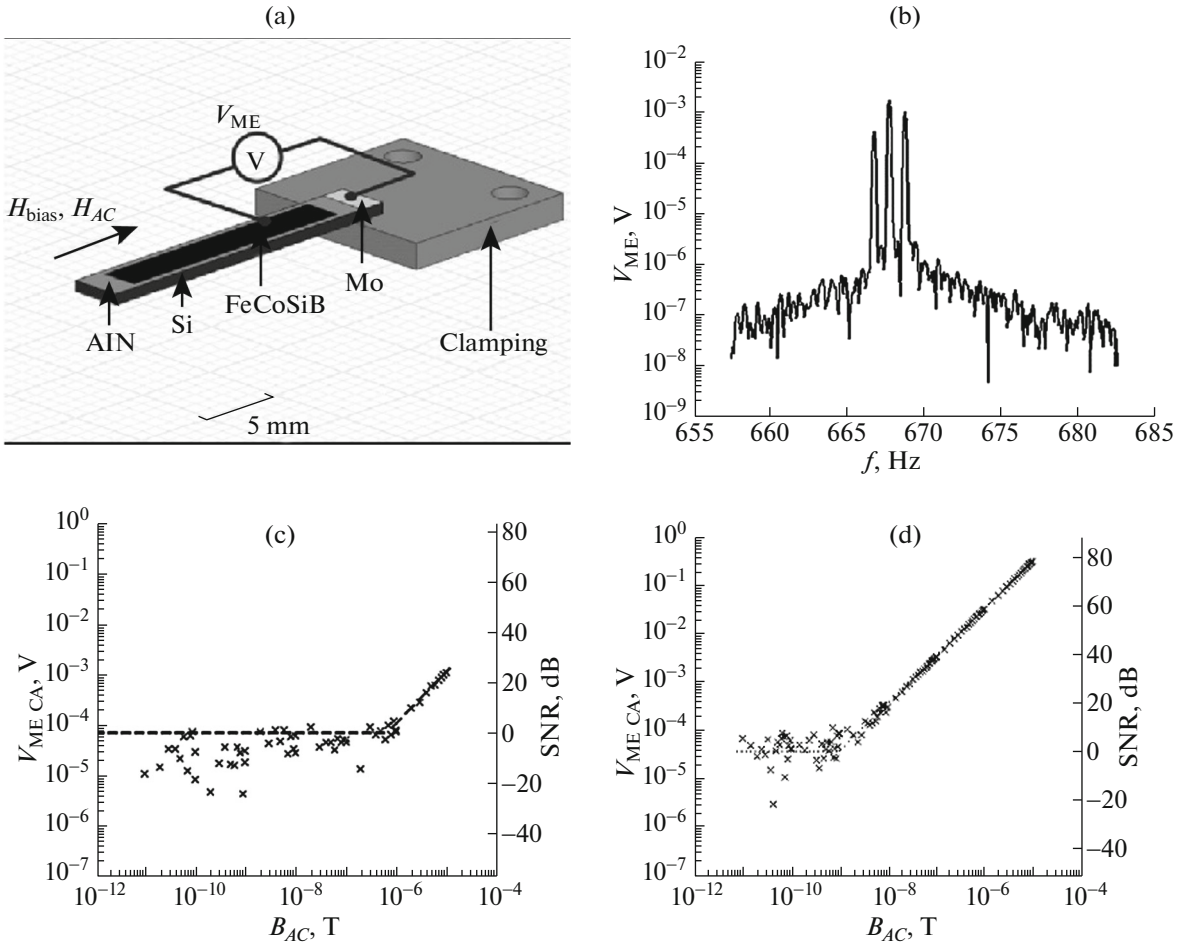

Fig. 27. Schematic image of the studied ME structure AlN/Metglas (a). The spectrum of the ME response of the sensor measured using the low-frequency-signal conversion technique (b). Modulation signal (average peak) and B_{AC} signal converted with an increase in the frequency (left- and right-side bands) at the output of the ME sensor are presented in the graph. The dependence of the ME signal and signal-to-noise ratio (SNR) on the amplitude of the modulating MF at a frequency of 1 Hz via direct measurement (c) and using the frequency-conversion technique (d) [24] (image and graphs copied with permission of Elsevier © 2021).

It is possible to decrease the contribution of external vibration noise using a differential structure with symmetrical response of the ME composite to the noise and asymmetrical to the useful signal. In [102], a ME structure with the asymmetrical location of Metglas relative to the piezoelectric layer was realized. As demonstrated in Fig. 28a, the ME structure consists of a PZT piezo fiber, to which ID electrodes are applied on two sides. Five Metglas layers are glued with epoxy resin to half of the length of the piezoelectric layer on the top and to the second half on the bottom. Such a structure is similar to those presented in Fig. 7 and has a *push-pull* configuration. Under the action of MF on the sample, the electric voltages $V_{ME,1}$ and $V_{ME,2}$ will have a different sign due to the opposite polarization (P_1 and P_2) in the piezoelectric layer, while the signal will be the same under the action of external noise. If $V_{ME,1}$ and $V_{ME,2}$ are connected sequentially, then the noise-induced symmetrical signal will be subtracted, while the useful ME response will be added [102].

Measurements of the equivalent magnetic-noise density for three cases of connection of a ME structure ($V_{ME,1} - 1$, $V_{ME,2} - 2$, and 1, 2 sequentially) are presented in Fig. 28b. The sequential connection of the output signals of the ME structure significantly increases the limiting sensitivity to MF. The equivalent density of the magnetic noise is 15.3 pT/Hz$^{1/2}$. This value is 1.4 times less than with a single connection of each ME sensor. The internal noise of the sensor prevails in region A in Fig. 28b. The external vibration noise created by equipment in the room, where the measurements of the ME sensor were carried out, is dominant in region B (2 Hz < f < 6 Hz). The greatest suppression of the external noise by the ME sensor (4.5 times) for successive connection is observed at the frequency 3.5 Hz. Laboratory sources of stochastic

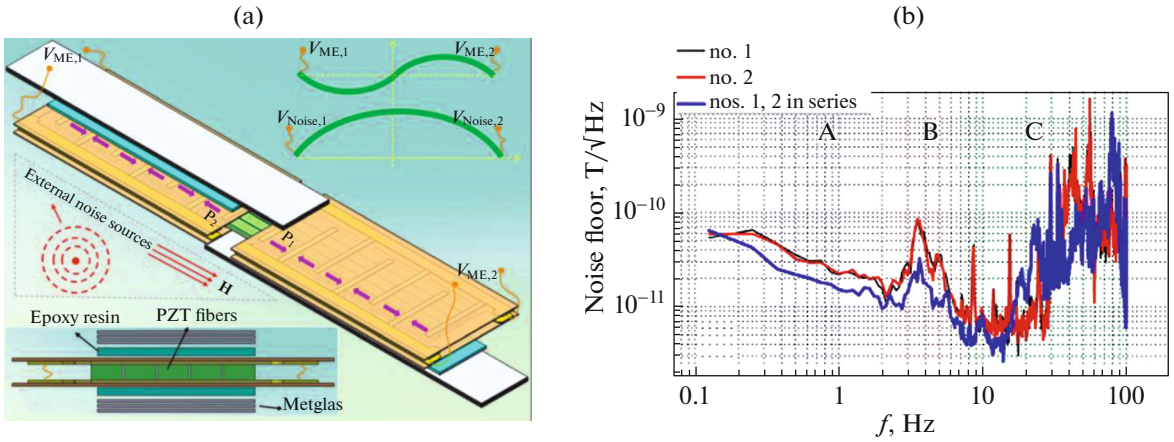

Fig. 28. Schematic image of the composite ME material and principle of operation under the influence of an external MF and external noise (a). Spectral-noise density of each of the ME samples and when connecting them successively in the range of frequencies 125 mHz < f < 100 Hz (b) [102] (image and graph copied with permission of AIP Publishing © 2021).

noise prevail in the frequency range C (6 Hz < f < 100 Hz).

In [103], a ME structure in the form of a cantilever symmetrically fastened using epoxy glue relative to the holder was suggested. Each individual ME structure is a silicon substrate, on one side of which a layer of magnetostrictive material is applied (an amorphous Metglas alloy was used in the device), while on the other side a layer of piezoelectric was applied (in this case, PZT). The upper cantilever was glued to the holder with the piezoelectric layer up; the second one, down (Fig. 29a).

When applying a magnetic field periodically changing in time to the device, ME structures bend in opposite directions, while the external vibration noise, on the contrary, always causes beam bending in the same direction. Thus, the vibration and magnetoelectric responses from a pair of symmetrical ME structures differ in phase, which allows efficient separation of these two components and partial compensation of the vibration noise to be performed.

A comparison was made of the limiting sensitivity of a single ME sensor with the suggested asymmetrical ME structure. The measurement of the ME response of a single sensor at the resonance frequency with a successive decrease in the amplitude of the modulating MF is presented in Fig. 29b. The limiting sensitivity was 5 pT at a frequency of 958 Hz, while the sensitivity for an asymmetrical ME structure increased to the value 500 fT (Fig. 29b). When applying the external wideband white noise from a speaker (Figs. 29b and 29c), the asymmetrical ME sensor demonstrated a sensitivity 4 times larger than the single ME sensor.

The need to coordinate the physical parameters of the used individual ME structures for efficient vibration-noise suppression is a disadvantage of such a device. Particularly, high demands are applied to the identity of sizes, weight, electromechanical and magnetomechanical characteristics of functional layers, and the quality of fastening in the holder. Due to the need to use several technological processes in the manufacture of structures, it is difficult to control accurately the matching of a pair of ME cantilevers according to the indicated parameters.

In [104], it was suggested to use an array of ME sensors to increase the sensitivity to MFs. Four sensors were connected in sequence to each other. The detected signal underwent amplitude and phase correction, while the signal was processed by the method of inverse dispersion, which allowed a sensitivity of 8.2 pT/Hz$^{1/2}$ to be reached at a frequency of 1 Hz. Massive sizes of the measuring system, and the time-consuming and continuous post-processing of the signal are disadvantages of the method.

The use of ID electrodes at the surface of the ferroelectric material in the composite ME material allows an increase in the output signal, thus increasing the sensitivity to MFs [105].

A significant potential for improving the parameters of ME devices based on Metglas and LN lies in the use of bidomain and bimorph LN crystals [106, 107] as the piezoelectric component. It is known that asymmetrical two-layer systems based on bimorph piezoelectrics consisting of two oppositely polarized layers along the thickness direction (Fig. 30) generate especially large ME coefficients with a bending resonance [26, 108]. At the same time, it is possible to use a low frequency bending electromechanical resonance for a significant increase in the ME effect. A schematic comparison of a single-domain and bimorph ME composite under the effect of a bending force is demonstrated in Fig. 30. In addition to an increase in the sensitivity at low frequencies and an increase in the ME coefficient, such a design is able to compensate partially the vibration and thermal noise [17, 30].

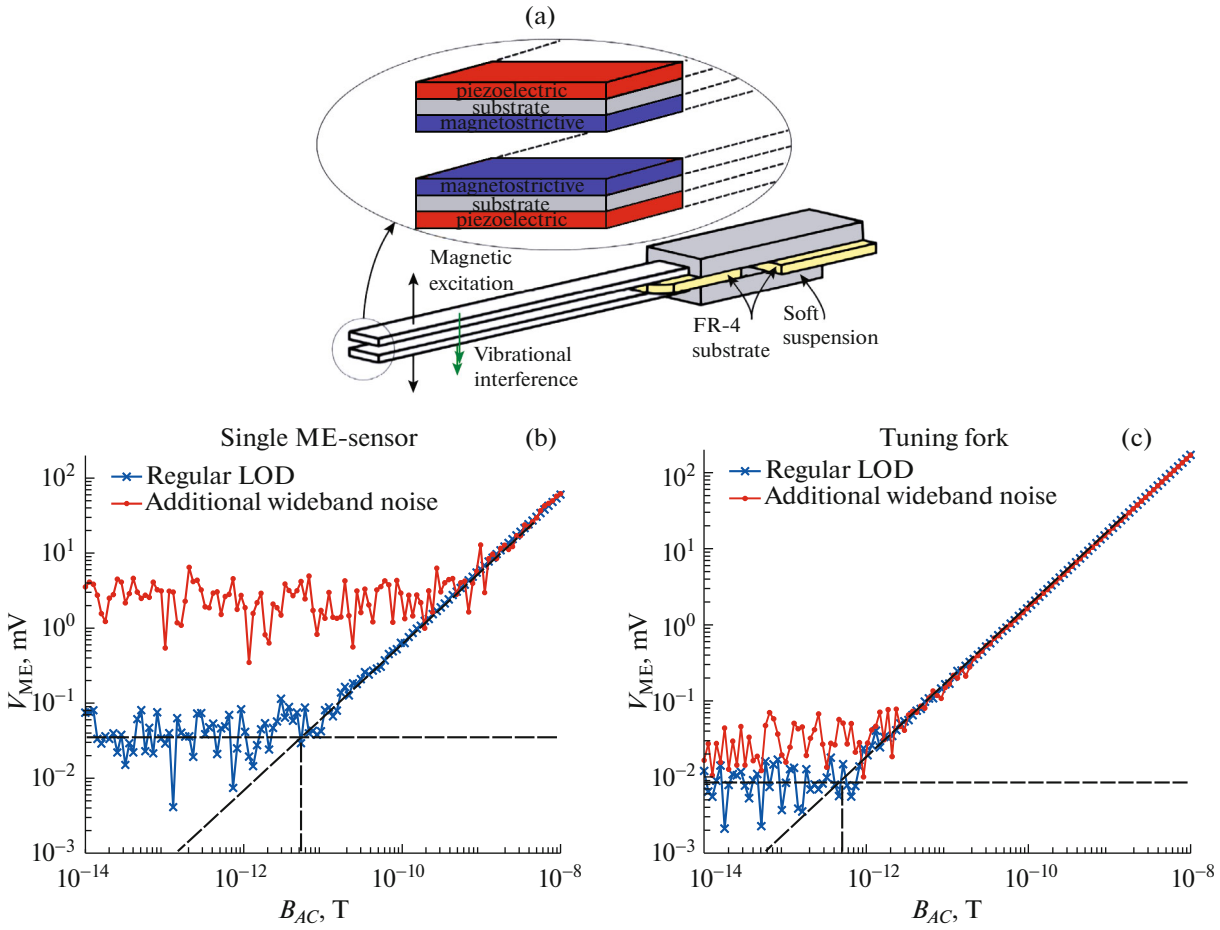

Fig. 29. Schematic image of the asymmetrical ME structure (a). Measurement of the limiting sensitivity depending on the amplitude of the variable MF (b) of a single ME sensor and (c) of an asymmetrical ME structure [103] (image and graphs copied with permission of Elsevier © 2021).

The use of a bidomain LN crystal as the piezoelectric part of a composite multiferroic excludes any losses associated with the sintering or gluing boundary. Lead-free crystal piezoelectrics also have low dielectric losses and multiple modes of anisotropic electromechanical resonance with a high mechanical quality factor [31, 110]. In addition, it was recently demonstrated that bidomain LN crystals have a linear bending deformation depending on the applied electric field [20]. The expected advantages are based on the amplification of low frequency bending modes as compared with similar modes in single-domain crystals and suppression of high-frequency contour modes. MF sensors based on bidomain LN crystals can be used to detect ultra-weak low frequency MF variations in a wide spectrum of devices [30, 31]: for noninvasive neurological interfaces, magnetoencephalography, magnetocardiography, the detection of magnetic anomalies and magnetic geological exploration.

In [109], bidomain LN crystals obtained using different technologies were studied in order for use in ME composites in application to sensors of ultra-weak MFs. Square LN plates of the $y + 128°$-cut with a size $10 \times 10 \times 0.5$ mm^3, in which bidomain structures were formed according to the diffusion-annealing technology (DAT) and light-annealing technology (LAT), were taken as the initial structures. To obtain the composite ME material, magnetostrictive amorphous Metglas alloy (the size $10 \times 10 \times 0.03$ mm^3) was applied to these structures using epoxy resin (Devcon epoxy 14260). ME samples based on single-domain

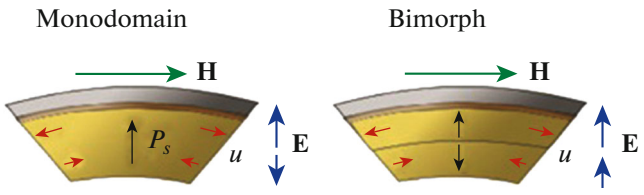

Fig. 30. Principle of operation of a ME bimorph and monodomain under the effect of bending force. **H** is the MF strength applied to the composite, and **E** is the resulting strength of the electric field in the piezoelectric material [109] (images copied with permission of IEEE © 2022).

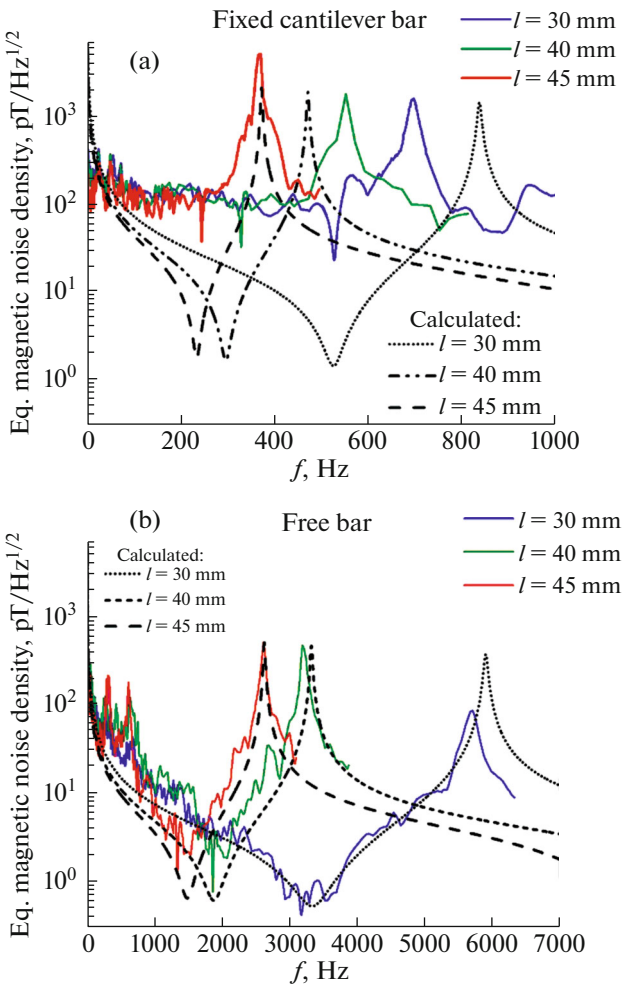

Fig. 31. Equivalent density of magnetic noise of composite ME materials (length l = 30, 40, and 45 mm) for two fastening modes: (a) cantilever fastening; (b) freely vibrating structure mode. The calculations of equivalent density of the magnetic noise for ME structures according to the dynamic model, in which only the thermal noise of the samples and input noise of the synchronous detector were taken into account, are also presented [119] (graphs copied with permission of IOP Publishing © 2022).

and bimorph LN crystals of the y + 128°-cut were also prepared for comparison. Bimorph samples with the structure "head-to-head" by means of the connection of two oppositely polarized LN crystals of the y + 128°-cut (0.25 mm thick each) were fabricated. ME measurements at a low frequency demonstrated that the maximal value of the $|\alpha_{E32}|$ coefficient is higher in bidomain samples as compared with the single-domain samples. $|\alpha_{E32}|$ is 2 times larger in the sample with the structure "tail-to tail" obtained by DAT than in the bimorph sample, as well as in the bidomain sample with the structure "head-to-head" (DAT). Dynamic measurements of the ME effect demonstrated that the largest ME coefficient 463 V/(cm Oe) corresponds to the bidomain sample with the structure "tail-to-tail" (DAT) at an antiresonance frequency of 30.8 kHz. This is consistent with low-frequency measurements of the ME coefficient. The minimum value of the equivalent magnetic noise was 524 fT/Hz$^{1/2}$ at the antiresonance frequency of the structure 30.8 kHz and 153 pT/Hz$^{1/2}$ at the frequency 1 kHz. These results were obtained for the best ME sample on the basis of a bidomain (DAT, "tail-to-tail") y + 128°-cut LN crystal/Metglas. The equivalent magnetic noise of the sample itself (which was 388 fT/Hz$^{1/2}$) was calculated for comparison. It is important to note that these values are comparable with the sensitivities obtained for ME materials on the basis of PZT and other piezoelectric ceramics [30, 111–116].

In [117], the realization of a possible advantage (anisotropy of LN crystals applied to ME sensors) was demonstrated. ME measurements of the structure on the basis of the bidomain y +140°-cut LN crystal/Metglas were carried out. The equivalent value of the noise and limiting sensitivity to the magnetic field of the ME sensor were also measured. The equivalent magnetic noise at the resonance frequency was 92 fT/Hz$^{1/2}$, which is a record for frequencies of less than 25 kHz [111, 113, 118] among composite multiferroics. The limit of MF detection without additional screening was δH = 200 fT at the resonance frequency 6.86 kHz.

However, the sensitivity to a low-frequency magnetic field for composite ME structures will be limited by external acoustic noises. This fact was experimentally studied in [119]. In order to decrease the working frequency and to increase the sensitivity of ME structures on the basis of bidomain LN crystals of y + 128°-cut/Metglas, it was suggested that rectangular structures with a length of 30, 40, and 45 mm, width 5 mm, and thickness 0.5 mm be studied. The measurements were carried out for two modes of fastening: cantilever and freely vibrating structure. The ME coefficient increases with the structure length and corresponds to the values 147, 395, and 440 V/(cm Oe) with the cantilever mode; the same dependence takes place for the freely vibrating structure mode: 179, 443, and 478 V/(cm Oe), respectively. The frequency dependence of the equivalent magnetic noise density for the composite ME materials is presented in Fig. 31.

The results of calculations describe well the experimental curves in the case of the freely vibrating structure mode with high frequency resonance modes, where the intrinsic thermal noise dominates against the background of the remaining noise. In the freely vibrating structure mode, the ME sample with the length 45 mm demonstrates an equivalent magnetic-noise value of only 1.2 pT/Hz$^{1/2}$ at the resonance frequency 1335 Hz. For the cantilever mode of sample fastening, the limit of sensitivity of the ME samples is an order of magnitude higher than that calculated due to the additional acoustic and low frequency noise introduced by the environment. However, the measured magnetic noise for the ME sample with the

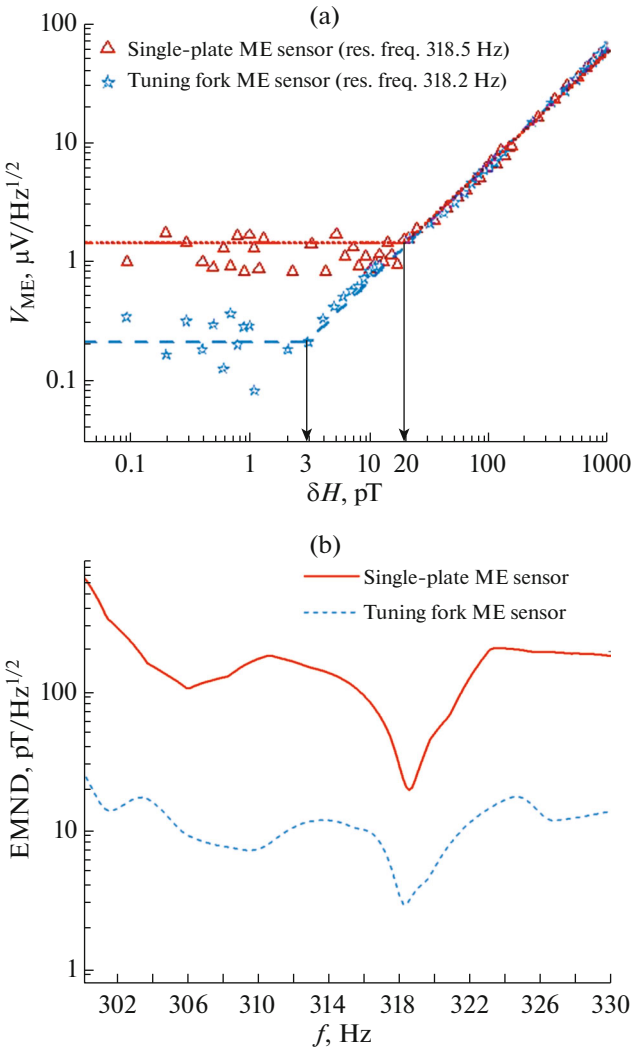

Fig. 32. Linear dependence of the ME voltage on an applied variable MF in the range from 0.1 to 1000 pT at the resonance frequency of the first wave of the ME sample (318.5 Hz) and ME tuning fork (318.2 Hz) at the optimal constant MF. Dashed horizontal lines demonstrated the level of noise, which determines the detection limit of the MF (a). Spectral density of the magnetic noise depending on the frequency (b) [120] (graphs copied with permission of Elsevier © 2021).

length 45 mm is still quite low (37 pT/Hz$^{1/2}$ at the resonance frequency 243 Hz).

In order to increase the sensitivity and to decrease the contribution of the parasitic vibration signal, the construction of a ME sensor on the basis of bidomain LN crystal of y + 128°-cut in the form of a tuning fork was developed in [120]. Unlike the previously suggested ME tuning fork, this design was fulfilled on a single piezoelectric-material crystal. Figure 32a demonstrates the sensitivity of a ME sensor in the form of a tuning fork to MFs as compared with the first wave of the ME structure in real conditions (without shielding from external noise). The limiting magnetic sensitivity of the tuning fork was 3 pT, while the wave

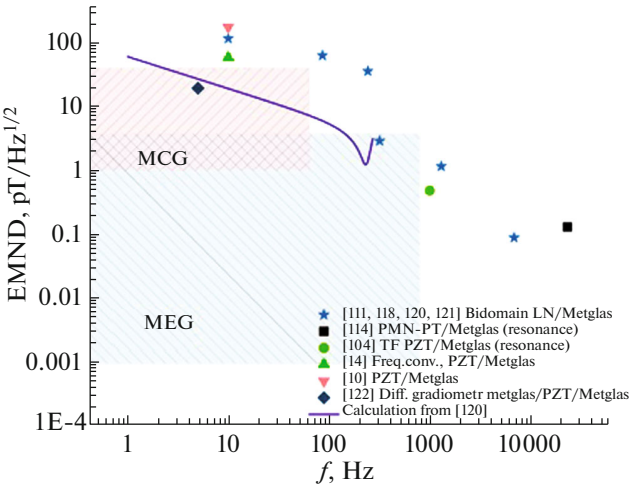

Fig. 33. Comparison of the sensitivity to MFs (EMND) depending on the signal frequency for different ME structures.

demonstrated the sensitivity ~20 pT. The density of voltage noise of the ME tuning fork was 0.2 μV/Hz$^{1/2}$, while for the wave it was 1.5 μV/Hz$^{1/2}$. The values of the spectral density of the magnetic noise for the ME tuning fork and the first wave of this structure are demonstrated in Fig. 32b.

The ability to suppress the noise varied from 7 to 25 times at nonresonance frequencies for the ME tuning fork as compared with a single ME sensor.

Comparison of the limiting sensitivity of the studied ME structures in the review, as well as with the required sensitivity to MF for magnetoencephalography and magnetocardiography techniques, is given in Fig. 33. Comparison of the sensitivity to a magnetic field (EMND) depending on the signal frequency is presented for the following ME structures: bidomain LN crystal/Metglas (asterisks [109, 117, 119, 120]), PMN-PT/Metglas [113] (square, sensitivity at the resonance frequency), asymmetrical ME sample PZT/Metglas [103] (circle, sensitivity at the resonance frequency), PZT/Metglas [14] (triangle, method for converting the frequency of the measured low-frequency signal), PZT/Metglas [10] (triangle, sensitivity at a nonresonance frequency), gradiometer Metglas/PZT/Metglas [121] (rhombus on the graph). The sensitivities required for the detection of biomagnetic signals for the magnetoencephalography (MEG) and magnetocardiography (MCG) techniques in the form of shaded regions are also presented in the figure. The calculation of EMND according to the dynamic model presented in [119] for a rectangular ME sample (LN y + 128°-cut/Metglas) in the form of a cantilever with a length of 45 mm corresponds to a solid curve.

The sensitivity of composite ME structures to MFs on the basis of lead-free piezoelectrics is not inferior in terms of the sensitivity to structures on the basis of

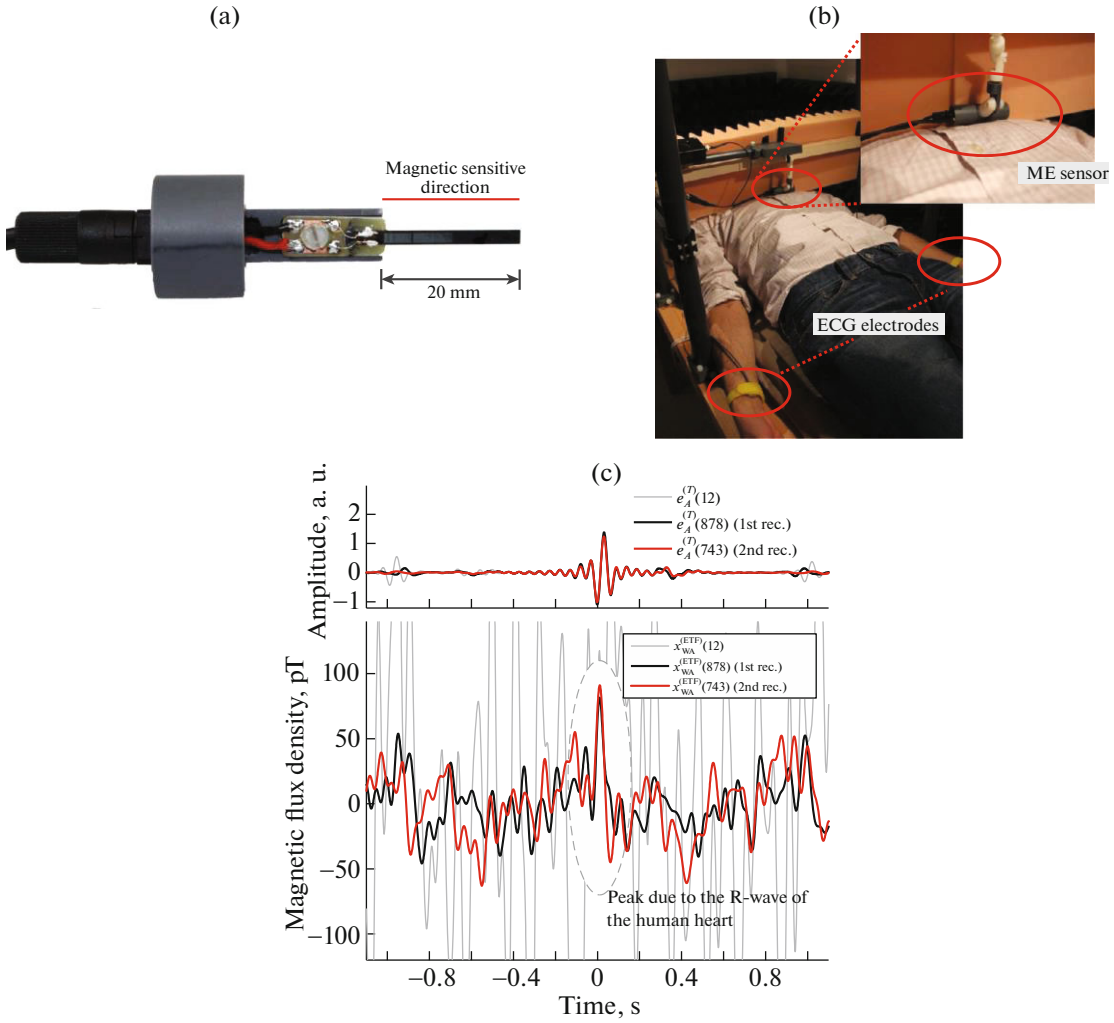

Fig. 34. ME sensor (a). Measuring device with a fastened ME sensor and ECG electrodes (b). Average results of R-wave measurement with the ME sensor as compared with an ECG (c). Different colors of the curves for ME measurements correspond to different number of signal averages [11] (image and graphs copied with permission of Elsevier © 2021).

PZT and PMN-PT. Composite multiferroics are also approaching the required sensitivity to use these sensors for studying ultra-weak MFs from the heart, brain and human nervous system.

Until recently, no work was published, in which the use of a ME sensor for the detection of biomagnetic fields from human organs was demonstrated. This was first demonstrated by a group of scientists from the University of Kiel in 2018. In [11], the simultaneous detection of the R wave from a QRS complex (depolarization of heart ventricles) when measuring the signal by an electrocardiograph (ECG) and a ME sensor. The general view of the sensor, a photo of the experiment, and the results of measurements with the ME sensor are presented in Fig. 34.

In order to improve the signal-to-noise ratio (SNR), the measurements were carried out by a frequency-conversion method and using ME-signal averaging. The signal from the ME sample was synchronized with the signal from the ECG. All measurements were carried out in a magnetically shielded room. The signal-averaging technique does not allow peaks before and after the heart R wave to be studied, which limits the possibilities of this method.

Further studies of ME materials for MF sensors should be focused on the search for new materials capable of decreasing the equivalent noise, as well as new designs and methods of measurement to increase the limiting sensitivity to MFs.

CONCLUSIONS

The largest ME effect is observed in layered composite multiferroics. The $L-T$ design (2–2) and its derivatives is the most popular one for composite ME materials. To achieve high values of the ME coefficient, it is necessary to select magnetostrictive materials with a large value of the piezomagnetic coefficient

and piezoelectric materials with a high value of the ratio of the piezoelectric coefficient to the dielectric permeability for the selected crystallographic direction and structure operation mode.

The analysis of works on the experimental study of the ME effect in composite multiferroics demonstrated that lead-free piezoelectric materials with low values of the piezoelectric coefficient can be useful in composite ME structures and demonstrate ME characteristics superior to composite multiferroics on the basis of lead-containing ferroelectrics.

From the point of view of the use of composite multiferroics in MF sensors, the temperature stability of the main characteristics of a piezoelectric material, absence of hysteresis of the mechanical-electrical properties, and relatively low production cost play a significant role. Lead-free LN, AlN, and LGT crystals satisfy almost all of these requirements. These materials have a large potential for their use in ME structures and devices on their basis.

The construction of composite multiferroics plays an important role in a decrease in the level of external noise when measuring the useful ME signal. A bimorph ME structure is able to suppress efficiently pyroelectric noise.

The creation of highly sensitive sensors of ultraweak MFs on the basis of composite multiferroics is a direction that is most promising and close to practical implementation. The lack of the necessity to cool such sensors is a significant technical advantage over superconducting quantum interference devices (used now for these purposes without an alternative). The study of magnetic signals from the human heart and brain will become possible upon reaching a high sensitivity of ME sensors to MFs with amplitudes from units of $fT/Hz^{1/2}$ to 100 $pT/Hz^{1/2}$ in the range of frequencies from mHz to 300 Hz.

The sensitivity of a ME sensor is limited, on the one hand, by its intrinsic noise, in which Nyquist thermal noise and the component of 1/f-noise dominate, and on the other hand, by external noise caused by vibrations of the piezoelectric, pyroelectric effect, and magnetic sources. Methods of dealing with these sources of noise and strategies for achieving a high sensitivity at low frequency were considered in the review.

The use of piezoelectric materials with the minimal possible value of the tangent of the dielectric-loss angle is one of the methods of increasing the sensitivity to MFs for ME structures. In order to exclude the effect of low-frequency vibration noise on a ME sensor, it is possible to use the low-frequency-signal conversion technique. This technique also allows to use more compact ME structures for the measurement of MFs. When measuring a MF using the modulation of a low-frequency signal, it is possible to achieve the MF sensitivity on 20 pT at a frequency of 1 Hz. However, the low-frequency-signal conversion technique has the following disadvantages: it is necessary to apply a modulating signal with a large amplitude to the ME sensor (from 2 to 10 Oe); it is necessary to know in advance what frequency the useful signal will have or scan permanently the range of acceptable frequencies for this signal, which will lead to a long measurement and signal processing time. It is possible to decrease the contribution of the external vibration noise using a differential structure with symmetrical response of the ME composite to the noise and asymmetrical response to the useful signal. For this, the construction of a ME sensor on the basis of a bidomain LN crystal of $y + 128°$-cut in the form of a tuning fork was developed. Such ME composite structure allowed a sensitivity to MF 7 times greater to be achieved than when using a single ME structure.

The magnetic signal from a human heart was for the first time recorded using a ME structure with the frequency-conversion method and using averaging of the ME signal from a composite multiferroic, as well as with synchronization of the signal from the ME sensor with ECG.

Possible steps in the development of composite ME structures for their use in MF sensors: a decrease in the linear sizes of sensitive elements, the search for new efficient designs to suppress parasitic signals, use of the MEMS technology to create an array of sensors for MF mapping, and improvement of detecting electronics.

FUNDING

This study was supported by the Russian Foundation for Basic Research (project no. 20-12-50229).

REFERENCES

1. W. Eerenstein, N. D. Mathur, and J. F. Scott, Nature (London, U.K.) **442** (7104), 759 (2006).
2. M. Fiebig, J. Phys. D **38** (8), R123 (2005).
3. M. M. Vopson, Crit. Rev. Solid State Mater. Sci. **40**, 223 (2015).
4. C.-W. Nan, M. I. Bichurin, S. Dong, et al., J. Appl. Phys. **103**, 31101 (2008).
5. M. Bichurin, D. Viehland, and G. Srinivasan, J. Electroceram. **19**, 243 (2007).
6. C. Tu, Z.-Q. Chu, B. Spetzler, et al., Materials (Basel) **12**, 2259 (2019).
7. H. Palneedi, V. Annapureddy, S. Priya, et al., Actuators **5**, 9 (2016).
8. J. Ma, J. Hu, Z. Li, et al., Adv. Mater. **23**, 1062 (2011).
9. G. Srinivasan, Ann. Rev. Mater. Res. **40**, 153 (2010).
10. V. Röbisch, S. Salzer, N. O. Urs, et al., J. Mater. Res. **32**, 1009 (2017).
11. J. Reermann, P. Durdaut, S. Salzer, et al., Measurement **116**, 230 (2018).
12. H. Lin, M. R. Page, M. McConney, et al., MRS Bull. **43**, 841 (2018).

13. K. Sternickel and A. I. Braginski, Supercond. Sci. Technol. **19**, S160 (2006).
14. S. Salzer, V. Röbisch, M. Klug, et al., IEEE Sens. J. **18**, 596 (2018).
15. V. Annapureddy, H. Palneedi, W.-H. Yoon, et al., Sens. Actuators, A **260**, 206 (2017).
16. J. Reermann, E. Elzenheimer, G. Schmidt, IEEE Sens. J., 1 (2019).
17. Z. Xing, J. Zhai, J. Li, et al., J. Appl. Phys. **106**, 24512 (2009).
18. A. A. Timopheev, J. V. Vidal, A. L. Kholkin, et al., J. Appl. Phys. **114**, 44102 (2013).
19. J. V. Vidal, A. A. Timopheev, A. L. Kholkin, et al., Vacuum **122**, 286 (2015).
20. A. S. Bykov, S. G. Grigoryan, R. N. Zhukov, D. A. Kiselev, S. V. Ksenich, I.V. Kubasov, M. D. Malinkovich, and Yu. N. Parkhomenko, Russ. Microelectron. **43**, 536 (2014).
21. Z. P. Xing, J. Y. Zhai, S. X. Dong, et al., Meas. Sci. Technol. **19**, 15206 (2008).
22. R. Jahns, H. Greve, E. Woltermann, et al., IEEE Trans. Instrum. Meas. **60**, 2995 (2011).
23. X. Zhuang, C. Cordier, S. Saez, et al., J. Appl. Phys. **109**, 124512 (2011).
24. R. Jahns, H. Greve, E. Woltermann, et al., Sens. Actuators, A **183**, 16 (2012).
25. J. R. Petrie, J. Fine, S. Mandal, et al., Appl. Phys. Lett. **99**, 043504 (2011).
26. L. Y. Fetisov, N. S. Perov, Y. K. Fetisov, et al., J. Appl. Phys. **109**, 53908 (2011).
27. Y. Zhang, G. Liu, M. Li, et al., J. Alloys Compd. **641**, 188 (2015).
28. Y. K. Fetisov, D. V. Chashin, A. G. Segalla, et al., J. Appl. Phys. **110**, 066101 (2011).
29. V. M. Petrov, M. I. Bichurin, K. V. Lavrentyeva, et al., J. Electron. Mater. **45**, 4197 (2016).
30. J. Zhai, Z. Xing, S. Dong, et al., Appl. Phys. Lett. **88**, 62510 (2006).
31. Y. J. Wang, J. Q. Gao, M. H. Li, et al., Phil. Trans. R. Soc. London, Ser. A **372**, 20120455 (2014).
32. J. Gao, J. Das, Z. Xing, et al., J. Appl. Phys. **108**, 84509 (2010).
33. I. V. Kubasov, M. S. Timshina, D. A. Kiselev, M. D. Malinkovich, A. S. Bykov, and Yu. N. Parkhomenko, Crystallogr. Rep. **60**, 700 (2015).
34. I. V. Kubasov, A. M. Kislyuk, A. V. Turutin, M. D. Malinkovich, and Yu. N. Parkhomenko, Russ. Microelectron. **50**, 571 (2021).
35. P. Debye, Z. Phys. **36**, 300 (1926).
36. Y. Wang, J. Hu, Y. Lin, et al., NPG Asia Mater. **2** (2), 61 (2010).
37. D. C. Lupascu, H. Wende, M. Etier, et al., GAMM-Mitt. **38**, 25 (2015).
38. J. Ryu, S. Priya, K. Uchino, et al., J. Electroceram. **8**, 107 (2002).
39. C.-W. Nan, Phys. Rev. B **50**, 6082 (1994).
40. W. Kleemann, J. Phys. D **50**, 223001 (2017).
41. R. E. Newnham, D. P. Skinner, and L. E. Cross, Mater. Res. Bull. **13**, 525 (1978).
42. R. E. Newnham, Ferroelectrics **68** (1), 1 (1986).
43. T. Xu, C. A. Wang, and C. Wang, Ceram. Int. **41**, 11080 (2015).
44. I. V. Lisnevskaya, T. Lupeiko, and K. Myagkaya, J. Compos. Mater. **51**, 507 (2017).
45. A. Alyeksyei, N. Jiang, Y. Jiang, et al., Phys. Status Solidi RRL **13**, 1800691 (2019).
46. S. Dong, J.-F. Li, and D. Viehland, Appl. Phys. Lett. **83**, 2265 (2003).
47. X. Zhuang, M. L. C. Sing, C. Dolabdjian, et al., IEEE Sens. J. **15**, 1575 (2015).
48. M. Li, A. Matyushov, C. Dong, et al., Appl. Phys. Lett. **110**, 143510 (2017).
49. G. Sreenivasulu, P. Qu, V. Petrov, et al., Sensors **16**, 262 (2016).
50. M. I. Bichurin, V. M. Petrov, R. V. Petrov, et al., in *High Sensitivity Magnetometers,* Ed. by A. Grosz, M. J. Haji-Sheikh, and S. C. Mukhopadhyay (Springer Int., Cham, 2017), p. 127.
51. C. Lu, P. Li, Y. Wen, et al., IEEE Trans. Magn. **50** (11), 1 (2014).
52. C. M. Leung, S. W. Or, S. L. Ho, et al., IEEE Sens. J. **14**, 4305 (2014).
53. M. Bichurin, R. Petrov, V. Leontiev, et al., Sensors **17**, 1271 (2017).
54. M. Zhang and S. Or, Sensors **18**, 588 (2018).
55. C. M. Leung, X. Zhuang, J. Xu, et al., Appl. Phys. Lett. **110**, 112904 (2017).
56. J. Zhai, J. Gao, C. de Vreugd, et al., Eur. Phys. J. B **71**, 383 (2009).
57. X. Zhuang, C. M. Leung, G. Sreenivasulu, et al., Appl. Phys. Lett. **111**, 163902 (2017).
58. J. Zhang, W. Zhu, D. Chen, et al., J. Magn. Magn. Mater. **473**, 131 (2019).
59. J. Zhai, J. Li, S. Dong, et al., J. Appl. Phys. **100**, 124509 (2006).
60. C. M. Leung, X. Zhuang, J. Li, et al., J. Phys.: Conf. Ser. **1407**, 012025 (2019).
61. S. Dong, J. Zhai, J. F. Li, et al., App. Phys. Lett. **93**, 103511 (2008).
62. G. Liu, P. Ci, and S. Dong, App. Phys. Lett. **104**, 32908 (2014).
63. J. Ryu, J.-E. Kang, Y. Zhou, et al., Energy Environ. Sci. **8**, 2402 (2015).
64. Z. Chu, V. Annapureddy, M. PourhosseiniAsl, et al., MRS Bull. **43**, 199 (2018).
65. W. Gao, R. Brennan, Y. Hu, et al., Mater. Today **21**, 771 (2018).
66. R.-M. Friedrich, S. Zabel, A. Galka, et al., Sci. Rep. **9**, 2086 (2019).
67. X. Xue, Z. Zhou, B. Peng, et al., Sci. Rep. **5**, 16480 (2015).
68. A. A. Bukharaev, A. K. Zvezdin, A. P. Pyatakov, and Yu. K. Fetisov, Phys. Usp. **61**, 1175 (2018)
69. J. Lou, D. Reed, M. Liu, et al., Appl. Phys. Lett. **94**, 112508 (2009).
70. N. X. Sun and G. Srinivasan, Spin **02**, 1240004 (2012).
71. Y. Yan, L. D. Geng, Y. Tan, et al., Nat. Commun. **9**, 4998 (2018).

72. A. S. Tatarenko and M. I. Bichurin, Adv. Condens. Matter Phys. **2012**, 1 (2012).
73. M. I. Bichurin, I. A. Kornev, V. M. Petrov, et al., Phys. Rev. B **64**, 94404 (2001).
74. G.-M. Yang, J. Wu, J. Lou, et al., IEEE Trans. Magn. **49**, 5063 (2013).
75. T. Nan, H. Lin, Y. Gao, et al., Nat. Commun. **8**, 296 (2017).
76. J. Xu, C. Leung, X. Zhuang, et al., Sensors **19**, 853 (2019).
77. J. Lou, M. Liu, D. Reed, et al., Adv. Mater. **21**, 4711 (2009).
78. M. Liu, Z. Zhou, T. Nan, et al., Adv. Mater. **25**, 1435 (2013).
79. G. V. Duong, R. Groessinger, M. Schoenhart, et al., J. Magn. Magn. Mater. **316**, 390 (2007).
80. J. Lu, D.-A. Pan, B. Yang, et al., Meas. Sci. Technol. **19**, 045702 (2008).
81. J.-P. Rivera, Eur. Phys. J. B **71**, 299 (2009).
82. R. Jahns, A. Piorra, E. Lage, et al., J. Am. Ceram. Soc. **96**, 1673 (2013).
83. J. H. Scofield, Am. J. Phys. **62**, 129 (1994).
84. J. Zhai, S. Dong, Z. Xing, et al., Appl. Phys. Lett. **89**, 83507 (2006).
85. K.-H. Cho and S. Priya, Appl. Phys. Lett. **98**, 232904 (2011).
86. J. Zhai, Z. Xing, S. Dong, et al., J. Am. Ceram. Soc. **91**, 351 (2008).
87. S. Dong, J. Zhai, F. Bai, et al., Appl. Phys. Lett. **87**, 62502 (2005).
88. S. Dong, J. F. Li, D. Viehland, et al., Appl. Phys. Lett. **85**, 3534 (2004).
89. S. Dong, J. Zhai, and J. Li, Appl. Phys. Lett. **89**, 252904 (2006).
90. C. R. Bowen, R. Stevens, L. J. Nelson, et al., Smart Mater. Struct. **15**, 295 (2006).
91. S. Dong, J. Zhai, Z. Xing, et al., Appl. Phys. Lett. **91**, 022915 (2007).
92. Y. Wang, J. Gao, M. Li, et al., Appl. Phys. Lett. **101**, 022903 (2012).
93. G. Sreenivasulu, L. Y. Fetisov, and Y. K. Fetisov, Appl. Phys. Lett. **100**, 52901 (2012).
94. H. Greve, E. Woltermann, H.-J. Quenzer, et al., Appl. Phys. Lett. **96**, 182501 (2010).
95. H. Greve, E. Woltermann, R. Jahns, et al., Appl. Phys. Lett. **97**, 152503 (2010).
96. S. Trolier-McKinstry and P. Muralt, J. Electroceram. **12**, 7 (2004).
97. K. Krupa, M. Józwik, C. Gorecki, et al., Opt. Lasers Eng. **47**, 211 (2009).
98. A. A. Bent and N. W. Hagood, J. Intell. Mater. Syst. Struct. **8**, 903 (1997).
99. D. Murzin, D. J. Mapps, K. Levada, et al., Sensors **20**, 1569 (2020).
100. S. Zuo, J. Schmalz, M.-O. Ozden, et al., IEEE Trans. Biomed. Circuits Syst. **14**, 971 (2020).
101. Y. Liu, J. Jiao, J. Ma, et al., Appl. Phys. Lett. **103**, 212902 (2013).
102. J. Li and D. Viehland, J. Appl. Phys. **118**, 214103 (2015).
103. S. Salzer, R. Jahns, A. Piorra, et al., Sens. Actuators, A **237**, 91 (2016).
104. Y. Shen, K. L. McLaughlin, J. Gao, et al., Mater. Lett. **91**, 307 (2013).
105. A. Piorra, R. Jahns, I. Teliban, et al., Appl. Phys. Lett. **103**, 32902 (2013).
106. V. V. Antipov, A. S. Bykov, M. D. Malinkovich, et al., Ferroelectrics **374**, 65 (2008).
107. V. Y. Shur, I. S. Baturin, E. A. Mingaliev, et al., Appl. Phys. Lett. **106**, 53116 (2015).
108. V. D. Kugel, G. Rosenman, and D. Shur, J. Appl. Phys. **78**, 5592 (1995).
109. J. V. Vidal, A. V. Turutin, I. V. Kubasov, et al., IEEE Trans. Ultrason. Ferroelectr. Freq. Control. **64**, 1102 (2017).
110. Rajaram D. Patil, Y. Chai, R. C. Kambale, et al., Appl. Phys. Lett. **102**, 62909 (2013).
111. X. Zhuang, M. L. C. Sing, C. Cordier, et al., IEEE Sens. J. **11**, 2183 (2011).
112. W. Yaojin, G. David, B. David, et al., J. Appl. Phys. **122**, 84509 (2015).
113. C. Zhaoqiang, S. Huaduo, S. Weiliang, et al., Adv. Mater. **29**, 1606022 (2017).
114. Y. Wang, M. Li, D. Hasanyan, et al., Appl. Phys. Lett. **101**, 92905 (2012).
115. F. Cong, J. Jie, M. Jiashuai, et al., J. Phys. D **48**, 465002 (2015).
116. J. Gao, Y. Shen, Y. Wang, et al., IEEE Trans. Ultrason. Ferroelectr. Freq. Control **58**, 1545 (2011).
117. A. V. Turutin, J. V. Vidal, I. V. Kubasov, et al., Appl. Phys. Lett. **112**, 262906 (2018).
118. C. Fang, J. Ma, M. Yao, et al., J. Magn. Magn. Mater. **423**, 106 (2017).
119. A. V. Turutin, J. V. Vidal, I. V. Kubasov, et al., J. Phys. D **51**, 214001 (2018).
120. A. V. Turutin, J. V. Vidal, I. V. Kubasov, et al., J. Magn. Magn. Mater. **486**, 165209 (2019).
121. Y. Shen, J. Gao, L. Shen, et al., Sens. Actuators, A **171** (2), 63 (2011).

Translated by A. Barkhash